SIX-PRONG EVENTS IN $\pi^- p$ INTERACTIONS AT 7.0 GeV/C

by

James E. Campbell

Thesis submitted to the Graduate Faculty of the

Virginia Polytechnic Institute

in partial fulfillment for the degree of

DOCTOR OF PHILOSOPHY

in

PHYSICS

APPROVED:

Chairman M. A. Ijaz

James A. Jacobs

Burns Macdonald

Kazuo Gotow

David Kaplan

June 1969

Blacksburg, Virginia

TABLE OF CONTENTS

ACKNOWLEDGEMENTS

The author is grateful to M. A. Ijaz for suggesting the problem and for his guidance and support throughout the experiment. Thanks are also extended to Drs. R. Adler, S. Almeida, and R. Arndt for their answers to many questions.

The help of the scanning and measuring staff throughout the experiment and of in the early stages of the experiment is appreciated.

Acknowledgement is made to the "Research Division" of V.P.I. for supporting the project.

LIST OF FIGURES

LIST OF TABLES

SECTION I

INTRODUCTION

A $\pi^- p$ experiment at 7.0 GeV/c incident momentum was run at the BNL 80-inch hydrogen bubble chamber in December, 1965. The pion beam was produced at the Brookhaven Alternating Gradient Synchrotron. The film was scanned on a machine built at V.P.I. and on an Italian-made Prevost scanning assembly. The measurements were made on an Itek film plane digitizer with a least count of 1 micron. We have analyzed events with the following final states

$$\pi^- p \rightarrow \pi^- \pi^- \pi^- \pi^+ \pi^+ p \quad (1)$$

$$\pi^- p \rightarrow \pi^- \pi^- \pi^- \pi^+ \pi^+ p\pi^0 \quad (2)$$

$$\pi^- p \rightarrow \pi^- \pi^- \pi^- \pi^+ \pi^+ \pi^+ n \quad (3)$$

One of the original purposes of this experiment was the study of multiple pion resonances. A good deal of interest was generated in multiple pion resonances when Focacci et al.[1] studied the reaction $\pi^- p \rightarrow pX^-$ using a missing mass spectrometer. In this experiment incident momenta of 3, 3.5, 4.5, 5, 6, 7, and 12 GeV/c were used. They reported many peaks in the X^- mass spectrum from 1600 - 2500 MeV/c^2 (R, S, T, U mesons) which decayed into 3 or more pions. There is as yet not a great deal of evidence for the R, S, T, and U mesons in the data gathered from bubble chamber experiments.

At about the same time Focacci et al. reported on the boson mass spectrum, Bettini et al.[2] reported evidence for a possible $\rho^0\rho^0$

resonance at 1.41 GeV/c^2 in the reaction $\bar{p}d \to \pi^+\pi^+\pi^-\pi^-\pi^- p$. More recently Biswas et al.[3] have reported a $\rho^0\rho^-$ mass enhancement at 1710 MeV/c^2 which is interpreted to be resonant.

The A_1 and A_2 mesons (peaks at 1080 and 1300 MeV/c^2 decaying largely into $\pi\rho$) have been reported in many places[4,5]. The so called $A^5_{1.5}$ (seen in the $\pi\rho$ mass spectrum at 1170 MeV/c^2) and the A^6_3 (1660 MeV/c^2 enhancement decaying principally via πf^0) have gained a fairly high level of confidence but could perhaps use further confirmation. In 1963 Abolins et al.[7] reported evidence for a $\pi\omega^0$ resonance at 1210 MeV/c^2. This enhancement was called the B meson and was believed for some time to be due to kinematic effects. The B meson has, however, been seen in $\bar{p}p$ annihilations at rest[8] where the kinematic effects are not present. The H enhancement, first seen in 1964[9] as a peak at 990 MeV/c^2 in the $(\pi\rho)^0$ mass spectrum has recently been interpreted as a kinematic effect.

The few examples above represent a large part of the reason for our study of six and seven body final states. Seemingly at odds with the search for resonances is the study of the statistical nature of these interactions.

For more than a decade it has been observed that the average value of the transverse momentum, $\langle p_t \rangle$, for secondaries is approximately constant in πN and NN collisions with incident particles from 6 GeV to cosmic ray energies. It has also been found that $\langle p_t \rangle$ decreases with the increasing multiplicity and increases with the mass of the particle.

Experimental p_t distributions have been fitted to various statistical

distributions with somewhat surprising success (see Section IV for references). In the simplest statistical predictions one assumes that the two colliding particles are lost in the interaction and thus an isotropic emission of secondary particles in the center of mass system is expected. In an actual collision process, however, the colliding particles create collective motions along the collision axis in the hadronic matter producing some forward and backward grouping in the center of mass angular distributions. Recently Hagedorn has combined statistical thermodynamics and relativistic kinematics in a model which is able to predict the constancy of $\langle p_t \rangle$ with incident energy, the dependence of $\langle p_t \rangle$ on the mass of the particle, and the shape of the p_t spectrum. We have fitted our p_t distributions to an expression derived in the Hagedorn model. The results of these fits are presented in Section IV. The total six prong cross section and partial cross sections for reactions (1), (2), and (3) are presented in Section III. Section V contains a discussion of the resonance production found in this study.

SECTION II

EXPERIMENTAL PROCEDURE

A. Scanning

The data analyzed was taken from 16 rolls of 70 mm film. The total data taken at the time of the experiment was 30 rolls of which 10 rolls were of such poor quality as to be considered unmeasurable. Each roll contained approximately 2000 frames. Each roll of film was scanned twice for six-prong events. In order to determine the scanning efficiency the following procedure was used:[10]

Let N_i be the number of events found by scanner i.

N_b be the number of events found by both scanners.

P_i be the probability for scanner i to find an event.

N be the total number of events that exist.

N_{ij} be the number of events found by i but missed by j.

Then $P_i = N_i/N$

$$N_{ij} = N_i(1-P_j)$$

giving $$P_j = \frac{N_i - N_{ij}}{N_i} = N_b/N_i$$

which determines the scanning efficiency for scanner j. The overall scanning efficiency is then the average of the individual scanning efficiencies. Using this procedure our scanning efficiency for six prongs was found to be 95%.

Scanning was done in a restricted fiducial volume. The fiducial

configuration and fiducial volume are shown in Figure 1. For each event the scanner recorded the frame number, event number, and other details such as stopping tracks and electron-positron pairs associated with the primary vertex. In addition the scanner often made decisions on the measurability of an event. If, for instance, the primary vertex of an event was badly obscured in any view, or there were too many tracks (number of beam particles > 20), the event was called unmeasurable. Approximately 3000 six-prongs were scanned.

B. Measuring

After scanning, the film was mounted on an Itek "Junior" film reader. The film reader utilizes optical encoders and has a least count of one micron. An IBM 526 keypunch is connected on line with the digitizer. The measuring of an event involved producing a master card containing the frame number, event number, date, and operator identification. To provide reference points for event reconstruction, the operator recorded on the master card the coordinates of fiducials 4a and 7a (points at the hydrogen-glass interface with precisely known positions. See Figure 1.) Following the master card were track cards containing the event, frame, track, and view numbers followed by coordinates of points along the track. The tracks were numbered in View 2 (see Figure 1 for camera configuration) and measured in the same order in all three views. Figure 2 shows some examples of track numbering. For an average track of 50 cm. or longer, 7 to 12 points were measured. For shorter tracks fewer points were recorded. In the case of very short tracks ($\leq$ 2 cm.) only two points were punched -

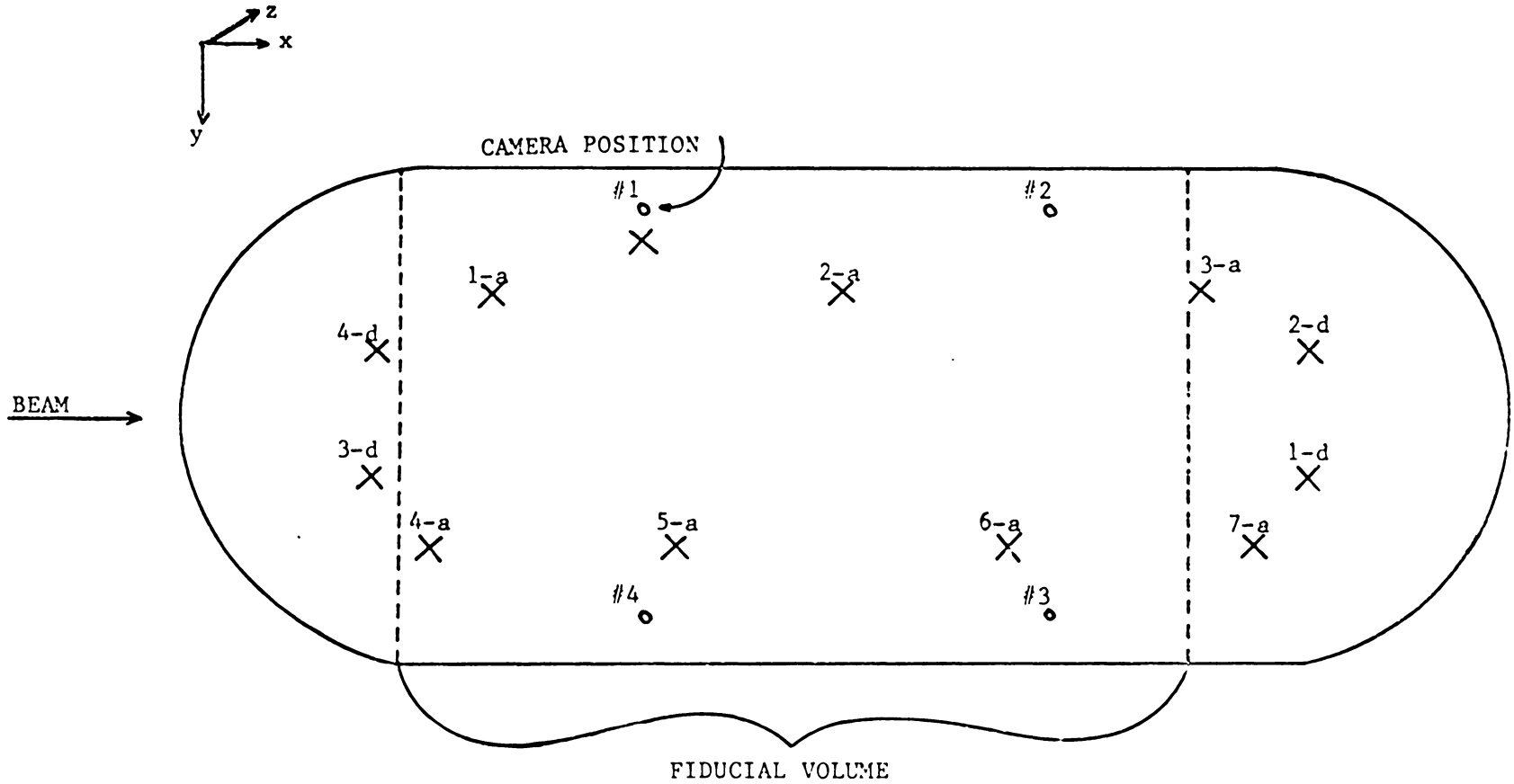

FIGURE 1. Bubble Chamber Fiducial and Camera Configuration

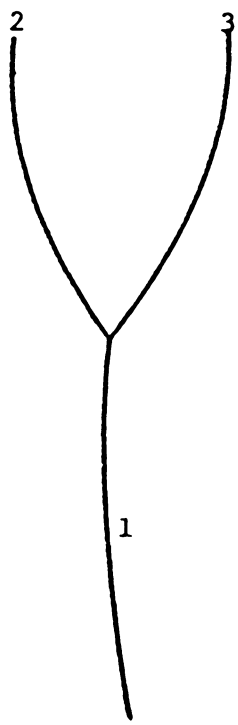

EVENT TYPE 22

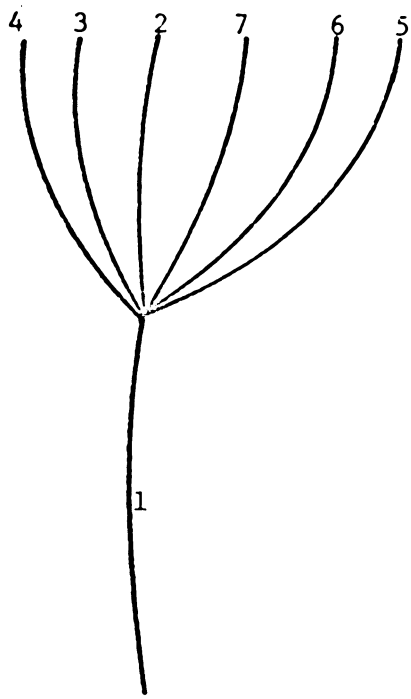

EVENT TYPE 26

FIGURE 2. Examples of Track Numbering

the vertex and the end point. An event was completed when all seven tracks (beam plus six secondaries) were measured in three views. In some cases (e.g. pictures too faint or vertex obscured by an electron) events were rejected as unmeasurable by the measuring operator. A total of 2250 events were measured from the scanned sample.

To determine the beam momentum several long beam tracks were measured. The corresponding beam momentum distribution is shown in Figure 3. The central value is about 6950 MeV/c with a spread of ±3%.

C. Reconstruction and Fitting

The events were reconstructed in the space of the bubble chamber by the Berkeley Three View Geometry Program (TVGP). To find the coordinates of a bubble in the chamber which produced an image on the film, TVGP first transforms and scales from the digitizer coordinate system to a coordinate system on the film having its origin on the camera axis for that view. In this system the light ray producing an image can be traced back into the chamber (see Figure 4). The coordinates (XO, YO) of a bubble in the chamber coordinate system (Figure 4) centered on the camera axis and at the hydrogen-glass interface are given by

$$XO = x(A + B(x,y) + C(x,y)*ZO)$$

$$YO = y(A + B(x,y) + C(x,y)*ZO)$$

where x and y are film coordinates centered on the camera axis. Of

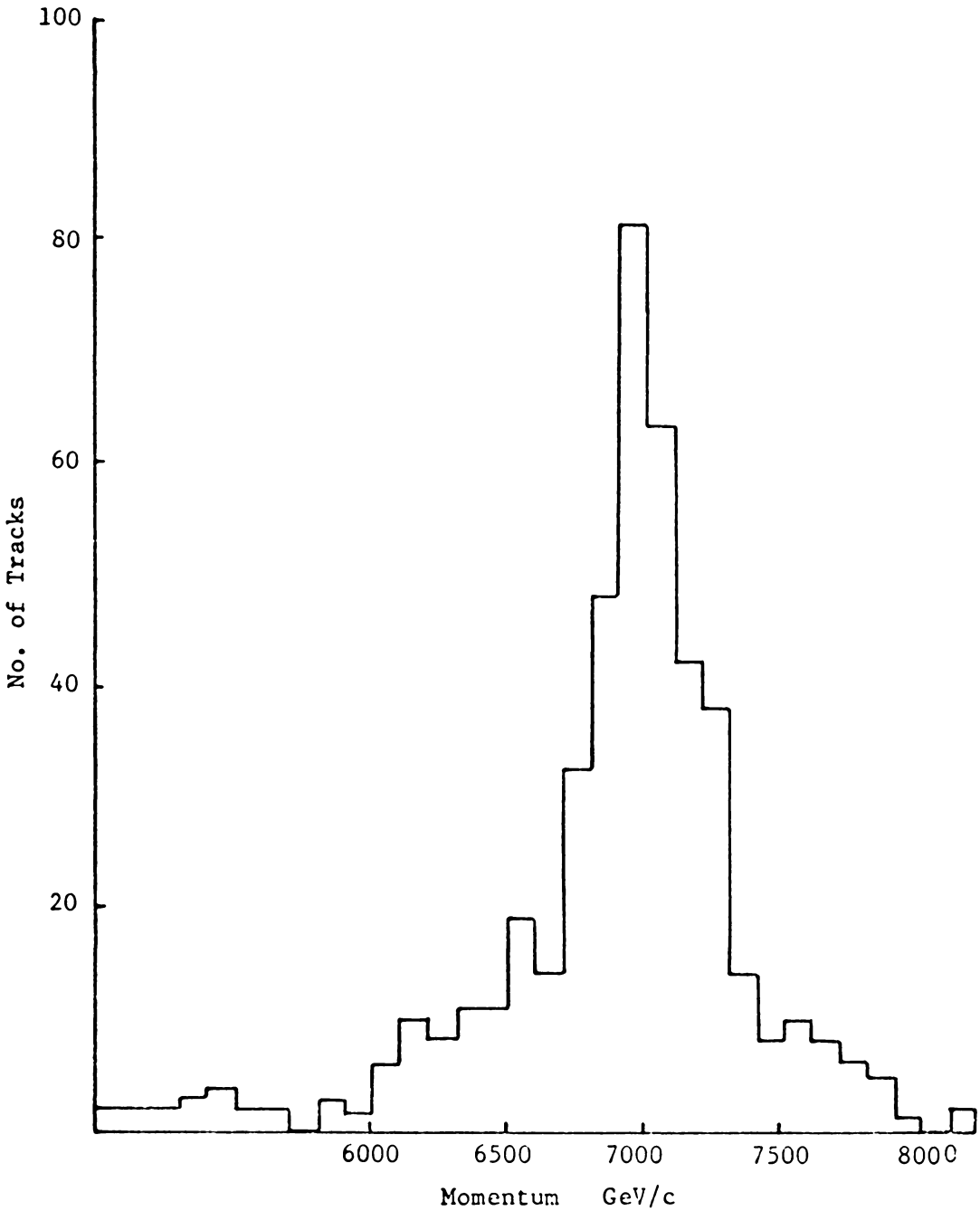

FIGURE 3. Beam Momentum

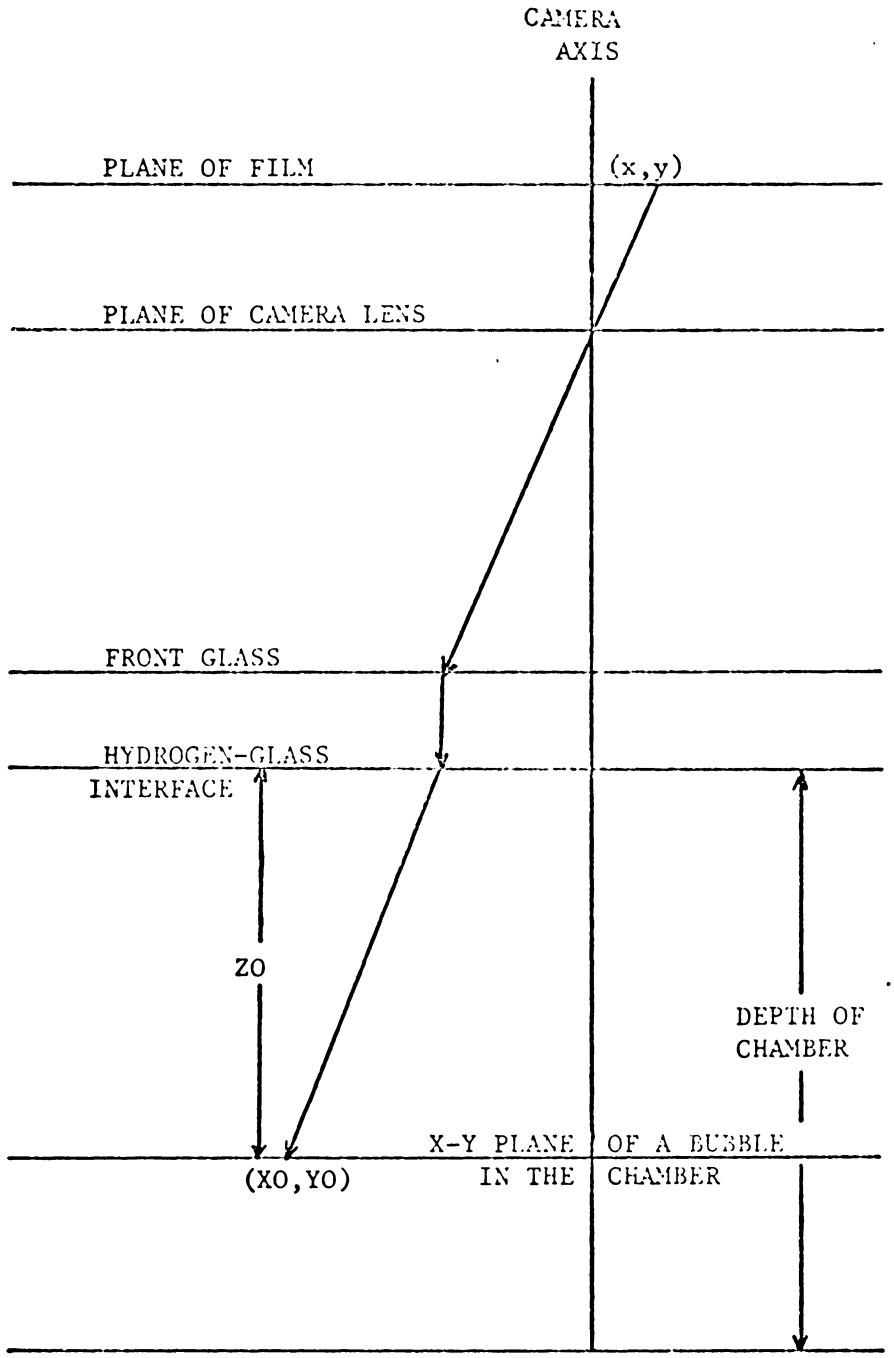

FIGURE 4. Transformation from Film to Bubble Chamber

course, ZO is not known at this point. If one can trace rays producing images of the same bubble in two different views back into the chamber, the intersection of these rays will give ZO. Once all the points for a track are found in the bubble chamber, they can be fitted to a circle allowing calculation of the azimuth and dip angles and the average momentum. The momentum is corrected for ionization loss back to the vertex. Thus for different masses the momentum will be different. About 90% of the events had all seven tracks reconstructed.

The TVGP output in the form of momenta, azimuth and dip angles, and the corresponding errors were recorded on tape to be used as input for the kinematic fitting program SQUAW. For an N body final state there are 3N measured quantities. At a vertex the four constraints of energy and momentum conservation must be satisfied. If, however, there are some unmeasured quantities to be determined (e.g. if there is a missing neutral particle) then the constraint equations must be used to calculate those unknowns. Thus in general there are L constraint equations where L may take on a value from 0 to 4. Hence in fitting a vertex, SQUAW minimizes the function

$$M = \sum_{i,j=1}^{3N} (X_i - X_i^m)\, G_{ij}\, (X_j - X_j^m) + 2\sum_{\lambda=1}^{L} \alpha_\lambda\, F_\lambda\, (X_i)$$

where the X_i are the fitted quantities, X_i^m are measured, and the F_λ are the equations of constraint. The normal equations are

$$\frac{\partial M}{\partial X_i} = 2\sum_{j=1}^{3N} G_{ij}(X_j - X_j^m) + 2\sum_{\lambda=1}^{L} \alpha_\gamma \frac{\partial F_\lambda}{\partial X_i} = 0, \qquad i=1,3N.$$

The remaining L equations are just the constraint equations

$$F_\lambda(X) = 0 \qquad \lambda = 1,L \ .$$

The equations can be solved for the X_i by iteration. The ETYPE subroutine in the SQUAW program was coded to fit reaction types (1), (2), and (3). Since any positive track could be a proton, reactions (1) and (2) involve three fits each. From the events reconstructed by TVGP, 57% were successfully fitted by SQUAW. The details of reconstruction and fitting are discussed in many places[11,12,13] and hence will not be discussed here.

SECTION III

EVENT CLASSIFICATION AND CROSS-SECTIONS

A. Event Classification

To classify events according to their final states the SQUAW fitted output of the measured events was examined along with the scanning information. The value of χ^2 (goodness-of-fit) was used as a criterion in accepting a particular SQUAW interpretation. An acceptable fit was one for which χ^2 was less than a predetermined limit and the fitted momenta agreed with the estimated ionization densities. The upper limit on χ^2 for the reactions (2) and (3) was chosen as 6.0 for the one degree of freedom. The upper limit on χ^2 for the reaction (1), where there are four degrees of freedom, was chosen as 25.0. This large value of χ^2 takes into account the various inaccuracies and approximations used in the kinematic fitting program.

Visual ionization checks are important in the classification of events. Figure 5 shows the variation of ionization density with momentum for pions and protons. The incident pion is treated as the reference of minimum ionization density, and the ionization of the outgoing tracks is compared with this standard. It is usually possible to distinguish a track if its ionization density is $\geq$ 1.5 times the minimum ionization. It can be seen from Figure 5 that pions and protons can be distinguished up to about 1.3 GeV/c. Above this momentum visual ionization checks become difficult. Consider a particle with 1.5 GeV/c momentum and a dip angle of 30°. If it

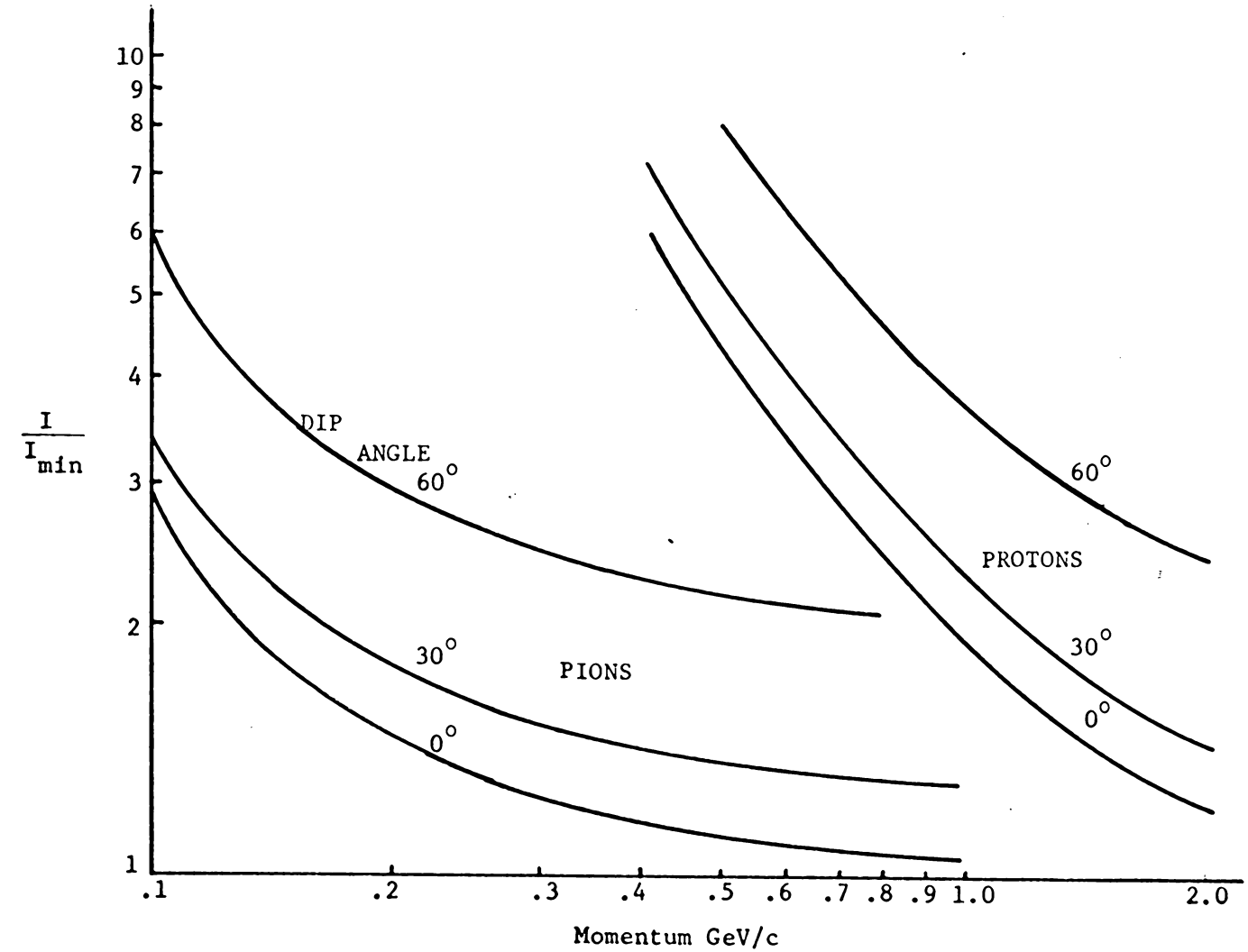

FIGURE 5. Ionization Versus Momentum for Pions and Protons.

were a pion its I/I_{min} would be 1.5, and if it were a proton its I/I_{min} would be 1.8. A visual ionization check would not be able to distinguish the difference. Most of the events yielded classification into reactions (1), (2) and (3) on the basis of χ^2 and visual ionization checks. When an event had acceptable fits to both reactions (2) and (3) and no choice could be made on the basis of ionization, then the fit with χ^2 lower than the other by a factor of 10 was chosen.

Figure 6 shows the missing mass distributions for reactions (1), (2), and (3). Events in reaction (3) are easily contaminated by events which fall into the categories $\pi^- p \rightarrow \pi^-\pi^-\pi^-\pi^+\pi^+ p + k(\pi^\circ)$, $k = 2,3...$, and $\pi^- p \rightarrow \pi^-\pi^-\pi^-\pi^+\pi^+\pi^+ n + k(\pi^\circ)$, $k = 1,2,....$. In order to remove these events we have retained in reaction (3) only those events having (missing mass)^2 between 0.4 and 1.5 $(GeV/c^2)^2$. Events classified on the above criteria were used in the further analysis of the data.

In order to calculate the partial cross sections it was necessary to classify remaining ambiguous events. The interpretation with the lowest χ^2 was chosen. If one believes that the momentum spectra of pions produced in high multiplicity interactions is the same for all kinds of pions (i.e. π^+, π^-, and π^0), then this fact can be used to resolve some of the ambiguities between reactions (1) and (2). In some cases SQUAW finds it easy to make a 1 constraint fit instead of a 4 constraint fit by adding to the six given charged tracks a slow neutral pion. In order to correct this problem we plotted the

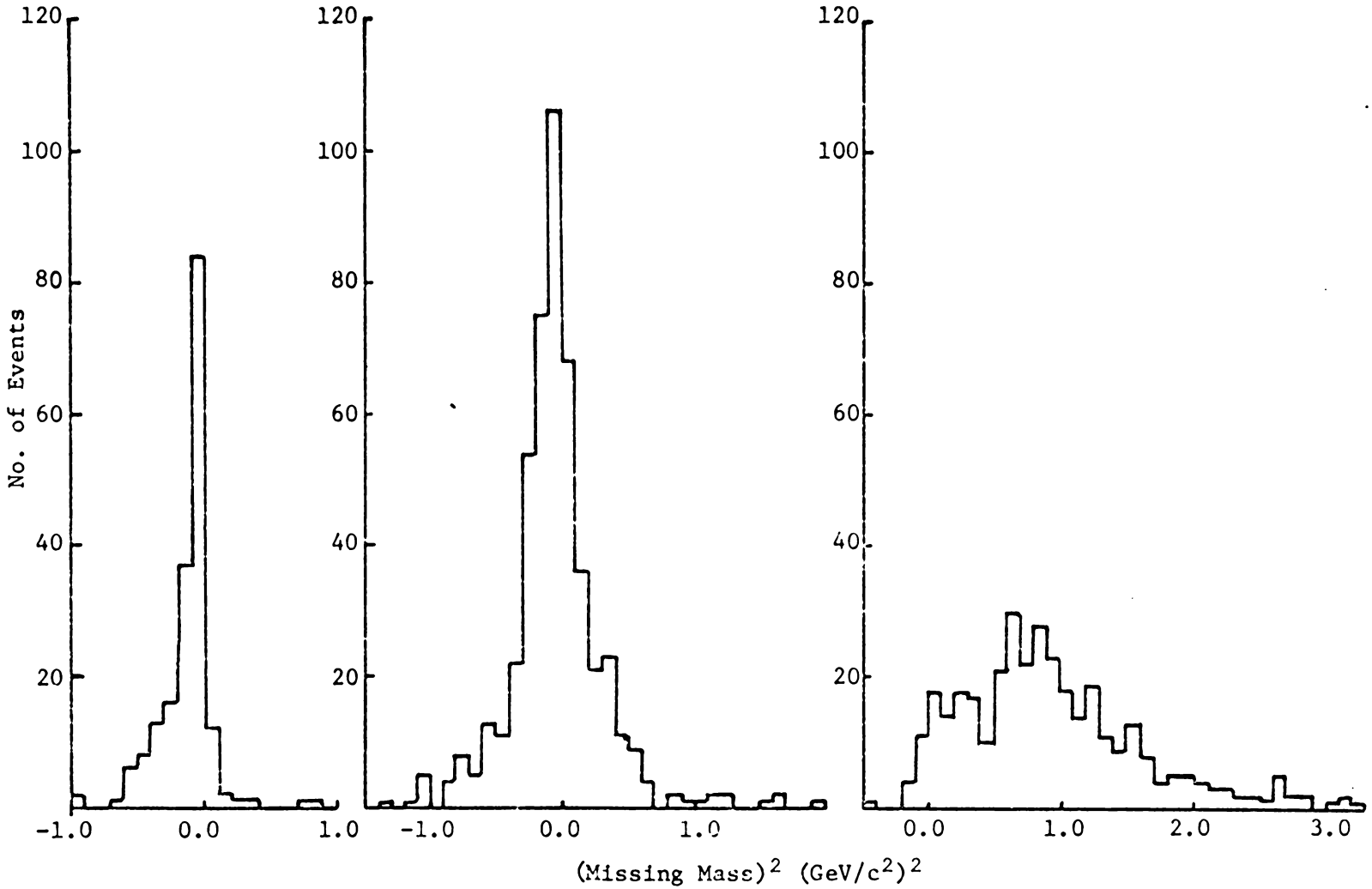

FIGURE 6. Missing Mass for Reactions (1), (2), and (3).

laboratory momentum distributions for the charged and neutral pions in reaction (2). We found that the number of neutral pions with lab momentum < 150 MeV/c was twice as large as the weighted number of charged pions. For the partial cross section calculations half the type (2) events having neutral pions with momenta < 150 MeV/c were treated as belonging to reaction (1).

B. Cross Sections

In order to calculate the total cross section for six prong events we used scanning data from 10 rolls of film. The total number of six-prong events found in this sample was corrected for losses due to scanning efficiency, and the total track length was corrected for losses due to interactions. We have assumed that the error in the number of six prong events is due to the statistical error of counting and the existence of four prong events with an electron-positron pair at the vertex. For the 1600 events used to calculate the cross section the statistical error is 2.5%. The error introduced by events with four prongs and an electron-positron pair at the vertex is about 2%. The resulting error in number of events is 3%.

There are two major sources of error in the total track length. One error is due to averaging the number of beam tracks entering the bubble chamber. This contributes about a 10% error. The other source of error in the track length is from muon and electron contamination in the beam. The contamination is estimated at 7%. After correcting the track length for this 7% loss we add a 4% error for contamination.

This gives an error in the total six prong cross section of 11%. The six prong cross section is calculated as 2.40 ± .27 mb.

The partial cross sections for reactions (1), (2), and (3) are given in Table I. The errors in the partial cross sections are due to estimated errors in classifying events and the error in the total cross section. Several six prong πp cross sections at different energies are shown in Figure 7. Our values are shown with arrows.

TABLE I

Total Six Prong Cross Section and Partial Cross Sections for Reactions (1), (2), and (3).

Final State	Number of Events	Cross Section(mb)
$\pi^-\pi^-\pi^-\pi^+\pi^+p$	211	0.22 ± 0.04
$\pi^-\pi^-\pi^-\pi^+\pi^+p\pi^0$	535	0.58 ± 0.09
$\pi^-\pi^-\pi^-\pi^+\pi^+\pi^+n$	230	0.24 ± 0.05
Others	1274	1.36 ± 0.14
Total	2250	2.40 ± 0.27

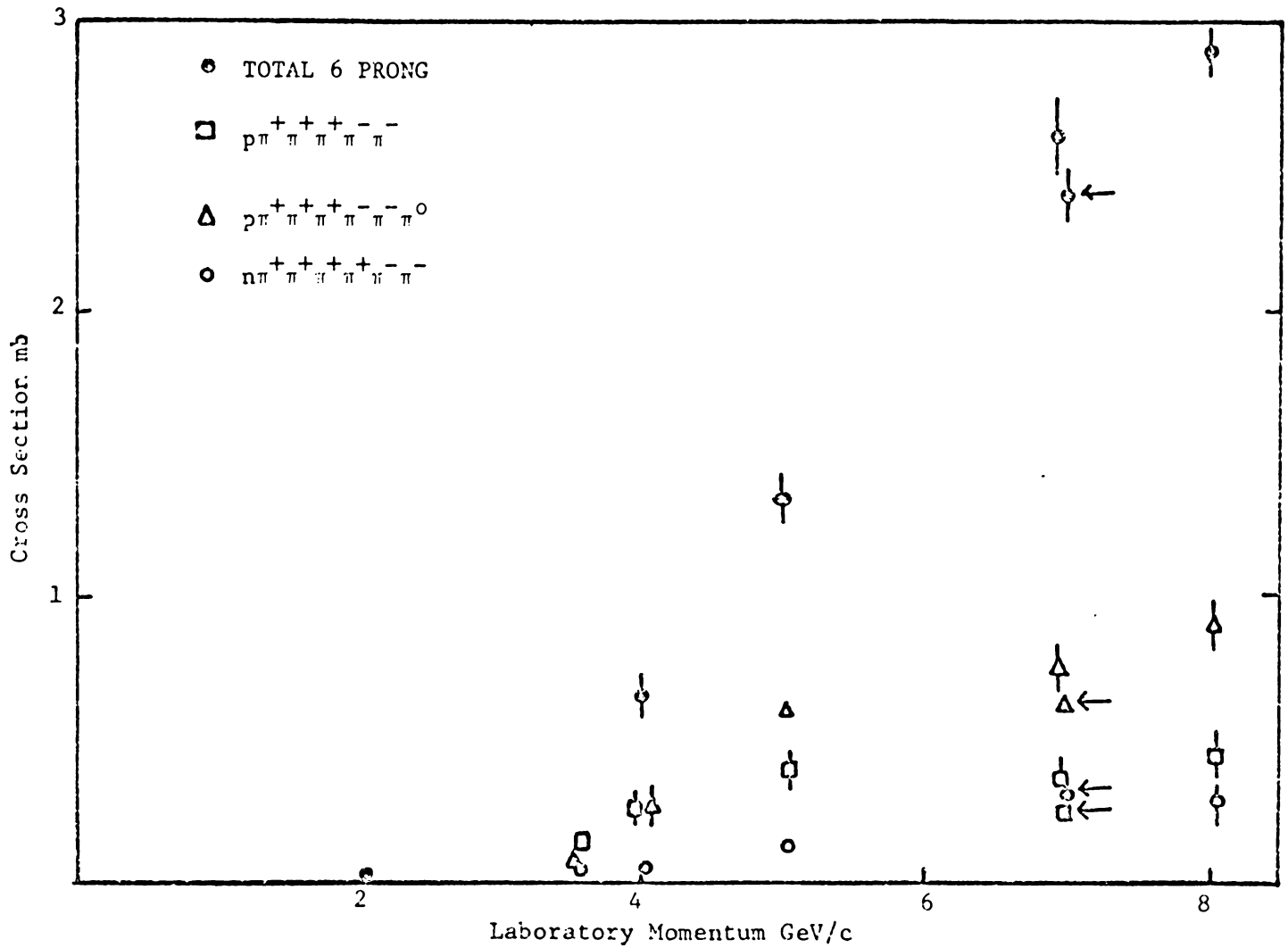

FIGURE 7. Some Six Prong πp Cross Sections

SECTION IV

COMPARISON WITH STATISTICAL MODEL PREDICTIONS

In a collision process given an initial state i the probability of producing a final state f having N particles with momenta between p_i and p_i+dp_i and energy between E_i and E_i+dE_i is given by Fermi's Golden Rule Number 2 as

$$P(i\to f) = C|\langle f|H_1|i\rangle|^2 \, d^3p_1 dE_1 d^3p_2 dE_2 \ldots . d^3p_N dE_N$$

$$\times \delta(E_1^2-p_1^2-m_1^2) \ldots . \delta(E_N^2-p_N^2-m_N^2)$$

$$\times \delta^3\left(\sum_{i=1}^{N} \vec{p}_i - \vec{P}\right) \delta\left(\sum_{i=1}^{N} E_i - E\right)$$

where H_1 is the interaction Hamiltonian, $\vec{P}$ is the total initial momentum, and E is the total initial energy. The delta functions assure conservation of energy and momentum and require that each particle satisfy the relation $E^2=p^2+m^2$. The total probability (or cross-section) for the final state f can be found by integrating over all final momenta and energies. For comparison with experimental results we assume that $\langle f|H_1|i\rangle$ is constant. The remainder of the expression can be written in the Lorentz invariant form

$$P(i\to f) = C' \prod_{i=1}^{N} [d^4q_i \delta(q_i^2-m_i^2)] \delta^4\left(\sum_{j=1}^{N} q_j - Q\right)$$

where q_i is the four momentum of the i^{th} particle and Q is the total initial four momentum. When integrated over all values of q_i (i=1,N), the expression above represents Lorentz invariant phase space.

$$R_N(\vec{P},E) = \int \prod_{i=1}^{N} [d^4q_i\ \delta(q_i^2-m_i^2)]\ \delta^4(\sum_{j=1}^{N} q_j - Q) \qquad (5)$$

A. Center of Mass Momentum Distributions

To find the momentum distribution predicted by phase space for the i^{th} particle it is necessary to evaluate $\frac{dR_N}{dp_i}(\vec{P},E)$. Noting that

$$\int dE_i\ \delta(q_i^2-m_i^2) = \int dE_i\ \delta(E_i^2-(p_i^2+m_i^2)) = \frac{1}{2E_i}$$

and evaluating equation (5) in the center of mass we get

$$R_N(0,E) = \int \frac{d^3p_N}{2E_N} \prod_{i=1}^{N-1} \frac{d^3p_i}{2E_i}\ \delta^3 \sum_{j=1}^{N-1} (\vec{p}_j - (-\vec{p}_N))\ \delta(\sum_{j=1}^{N-1} E_j - (E-E_N)) .$$

Which is just

$$R_N(0,E) = \int \frac{d^3p_N}{2E_N} R_{N-1}(-\vec{p}_N, E-E_N) \quad . \qquad (6)$$

Since $R_{N-1}(-\vec{p}_N, E-E_N)$ is invariant it may be evaluated in the center of mass of the N-1 particles to give

$$R_N(0,E) = \int \frac{d^3p_N}{2E_N} R_{N-1}(0,E_{N-1}) \qquad (7)$$

where E_{N-1} is the effective mass (total energy of the N-1 particles in their center of mass) of the N-1 particles. To find the momentum distribution of the N^{th} particle one merely omits the integration over p_N. Thus

$$\frac{dR_N(0,E)}{dp_N} = \frac{C\ p_N^2}{E_N} R_{N-1}(0,E_{N-1}) \qquad (8)$$

The center of mass momentum distributions for pions from reactions (1), (2), and (3) are shown in Figure 8. The nucleon momentum distributions are shown in Figure 9. The curves represent phase space predictions. There is fair agreement with phase space.

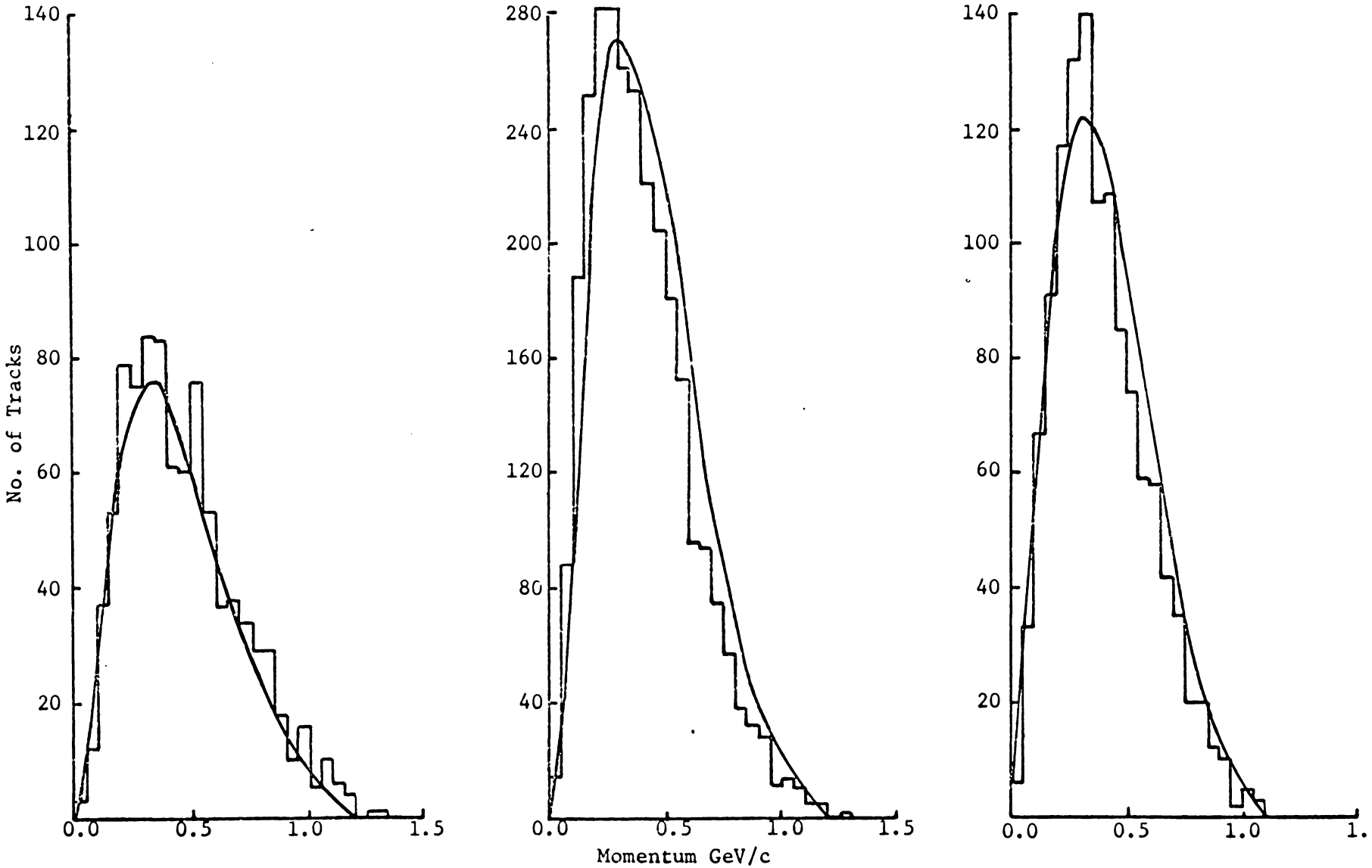

FIGURE 8. CM Momentum Distributions for Pions from Reactions (1), (2) and (3)

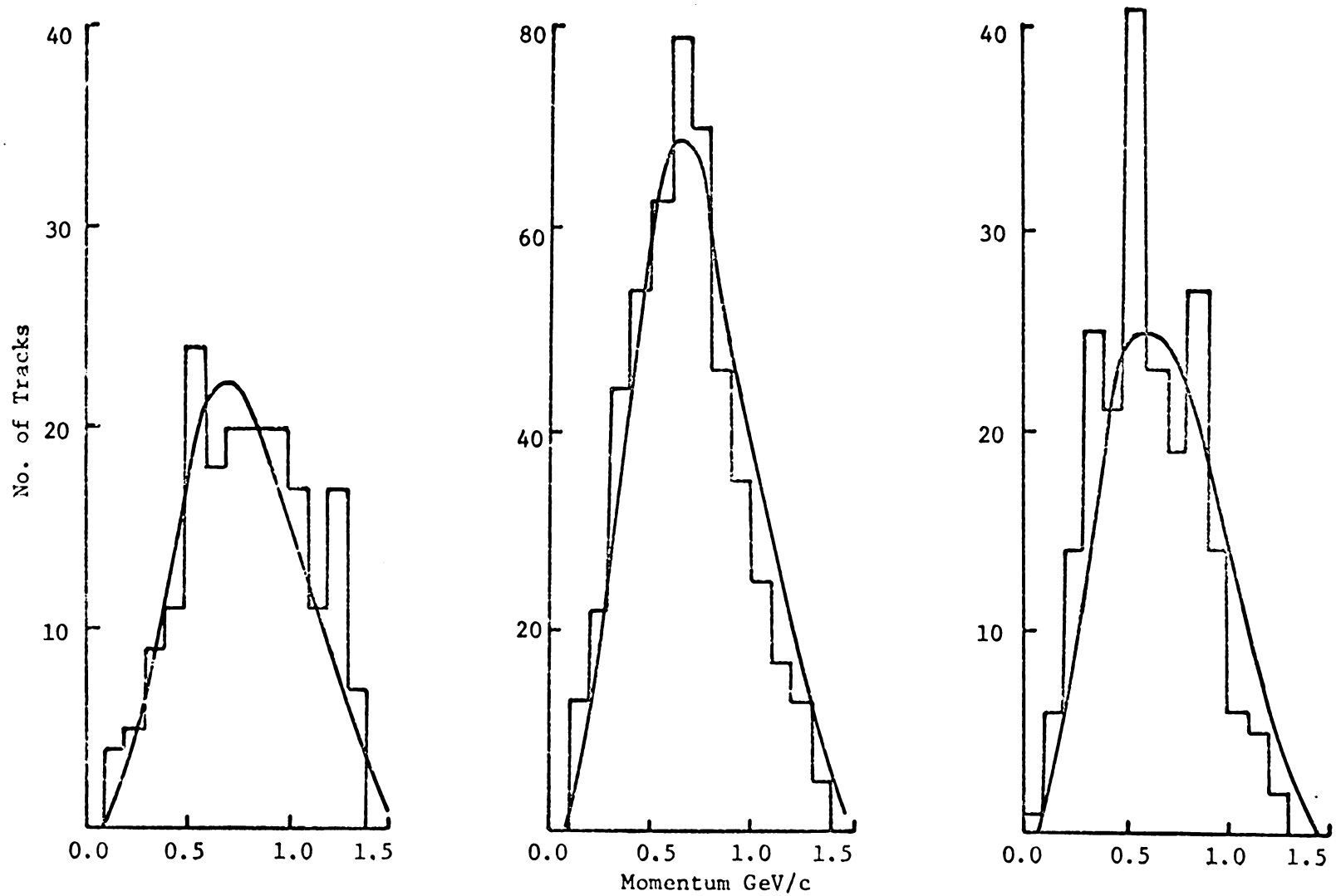

FIGURE 9. CM Momentum Distributions for Nucleons from Reactions (1), (2), and (3).

B. Transverse Momentum Distributions

It has been known for over a decade that the mean value of the transverse momentum $\langle p_t \rangle$, in high energy secondaries is nearly constant over a wide range of incident particle momenta. Initially the lack of significant variation of $\langle p_t \rangle$ over a wide range of incident energy lead physicists to believe that it held little information about the details of high energy interactions. This attitude began changing when Bigi et al.[15] showed that $\langle p_t \rangle$ increases with the particle's mass. A recent tabulation of the variation of $\langle p_t \rangle$ with the mass of the particle is given in Figure 10-a. There is also a noticeable variation of $\langle p_t \rangle$ with the primary energy (though slight for incident energy $\geq$ 6 GeV) as can be seen for pions and nucleons in Figures 10-b and 10-c. It has also been found that at a given primary energy $\langle p_t \rangle$ decreases with increasing multiplicity.

Recently many authors[16,17] have fitted p_t spectra to various analytical expressions. Imaeda[18] has assumed that in high energy, high multiplicity events the momentum distributions are given by Fermi's distribution for baryons and Planck's distribution for mesons. The distributions are given by

$$R_{\pm}(p)d^3p = A \frac{d^3p}{e^{E/\tau} \pm 1} \tag{9}$$

where + (-) signifies the Fermi (Planck) distribution. Here $\tau = kT$ where k is the Boltzmann constant and T is the temperature.

$$R_{\pm}(p)d^3p = Ad^3p \left[\sum_n (\pm 1)^{n+1} e^{-nE/\tau}\right]$$

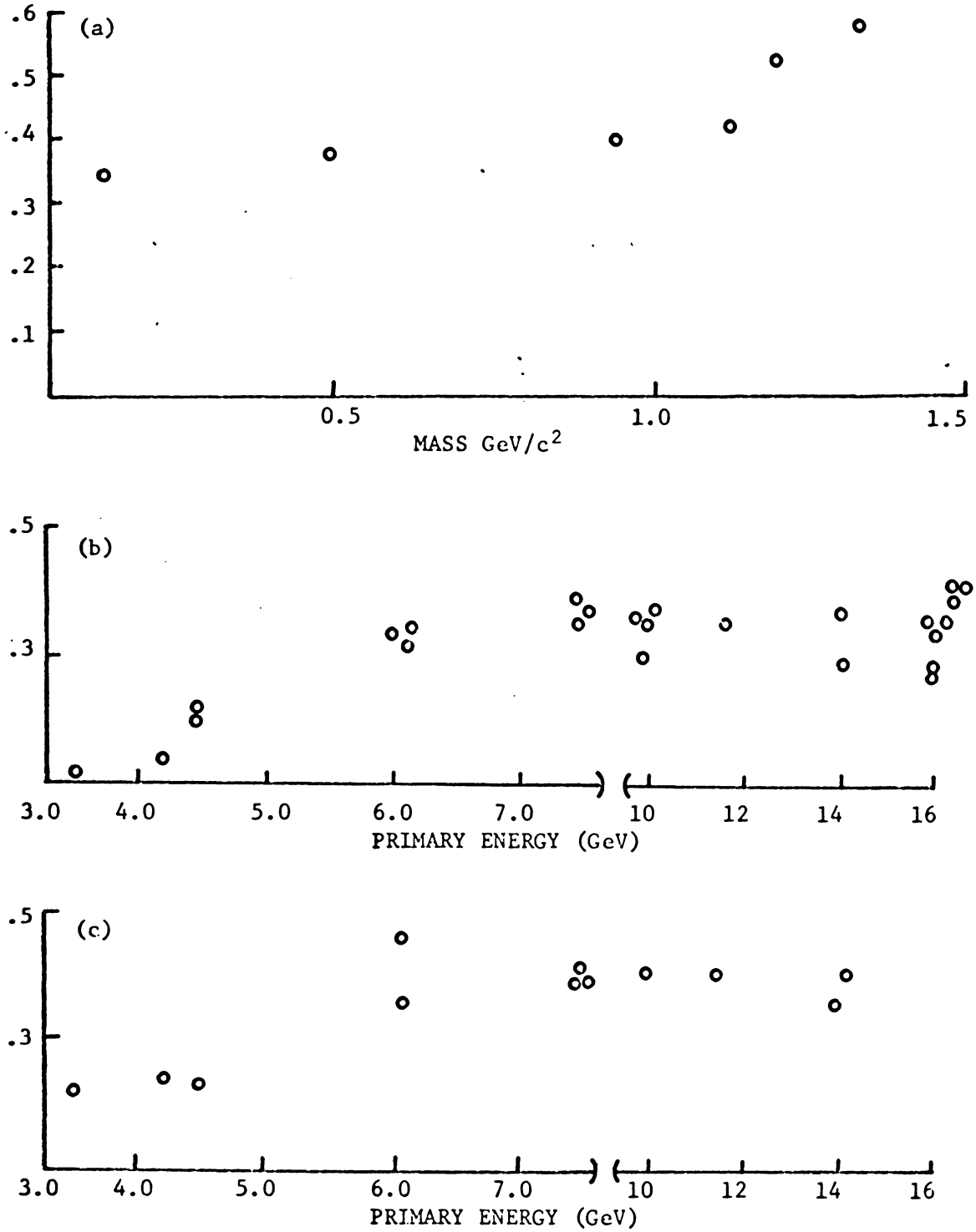

FIGURE 10. -a. Variation of $\langle p_t \rangle$ with Mass

-b. Variation of Pion $\langle p_t \rangle$ with incident Momentum

-c. Variation of Proton $\langle p_t \rangle$ with Incident Momentum

Now $K_{\frac{1}{2}}(x) = \sqrt{\pi/2x}\ e^{-x}$ (modified Bessel function of the second kind).

Thus

$$R_{\pm}(p)d^3p = Ad^3p\ [\Sigma(\pm 1)^{n+1}\ \frac{\sqrt{2nE}}{\sqrt{\pi\tau}}\ K_{\frac{1}{2}}\ (\frac{nE}{\tau})]$$

To find the p_t distribution integrate over p_l (longitudinal momentum) and ϕ. Hence

$$R_{\pm}(p_t)dp_t = Bp_t dp_t \int_0^{\infty} dp_l\ [\Sigma(\pm 1)^{n+1}\ \frac{\sqrt{2nE}}{\sqrt{\pi\tau}}\ K_{\frac{1}{2}}\ \left(\frac{n\sqrt{p_l^{\,2}+y^2}}{\tau}\right)$$

where $y^2 = p_t^{\,2} + m^2$. To perform the integration let $x = \sqrt{p_l^{\,2}+y^2}$ and $z = x/y$.

Then

$$R\pm(p_t)dp_t = Bp_t dp_t\ \Sigma(\pm 1)^{n+1}\ \frac{\sqrt{2n}}{\sqrt{\pi\tau}}\ y^{3/2} \int_1^{\infty} \frac{z^{3/2}dz}{\sqrt{z-1}}\ K_{\frac{1}{2}}(az),\ a = \frac{ny}{\tau}\ .$$

Integrating[19]

$$R\pm(p_t)dp_t = Bp_t dp_t\ \Sigma(\pm 1)^{n+1}\ y\ K_1\ (\frac{ny}{\tau}) \qquad (11)$$

Let R_+ be Planck distribution (PD) and R_- be Fermi distribution (FD).

Several other commonly used distributions can be derived from Equation (11) by making appropriate approximations. If $E/\tau >> 1$ (actually $E/\tau \geq 4$ will do which is satisfied by baryons and K mesons) then

$$R'(p)d^3p \simeq Ad^3p\ e^{-E/\tau} \qquad (12)$$

which integrates over p_l to give

$$KD \equiv Ap_t y\ K_1\ (\frac{y}{\tau})\ dp_t \qquad (13)$$

If one makes the further approximation $p^2/m^2 << 1$ then $E \simeq m + p^2/2m$ and equation (12) becomes

$$R(p)d^3p \simeq Ad^3p\ e^{-(m + p^2/2m)/\tau}.$$

Integrate over p_l to get the Boltzmann distribution (BD)

$$BD = \frac{2p_t}{\alpha}\ e^{-p_t{}^2/\alpha^2}\ dp_t\ . \tag{14}$$

Finally the linear distribution (LD) is given by

$$LD = \frac{p_t}{p_o}\ e^{-p_t/p_o}\ dp_t \tag{15}$$

which can be obtained from Equation (12) by assuming that $p_t >> p_l$ and $E \simeq p_t + p_l + m$. From the approximations made above one would expect BD to give better results when applied to baryons whereas LD should be applied to pions.

Friedlander[20] has fitted LD and BD to baryon p_t spectra and found good fits using BD but poor fits with LD. In order to fit secondary pion spectra to BD, Friedlander found it necessary to superimpose two BD's to get the form

$$f(p_t)dp_t = p_t dp_t\ [\frac{1-A}{\sigma_1{}^2}\ e^{-p_t^2/2\sigma_1^2} + \frac{A}{\sigma_2{}^2}\ e^{-p_t/2\sigma_2^2}] \tag{16}$$

with σ_1 and σ_2 differing widely. A possible explanation for the two components is that one is due to produced pions and the other component is due to isobar decay. It should be noted, however, that Friedlander puts his data into three groups: one with primary energy (E) < 6 GeV, a second with 6 GeV $\leq$ E < 30 GeV, and a third with E $\geq$ 30 GeV.

Lehar et al.[21] have fitted secondary pions from πN collisions at 7.0 GeV in emulsions to LD, BD, and PD. They find no significant difference in the quality of the fits as determined by χ^2. Lehar et al. find experimentally that $\langle p_t \rangle = 0.299 \pm 0.10$ GeV/c. From the fits LD

find experimentally that $\langle p_t \rangle = 0.299 \pm 0.10$ GeV/c. From the fits LD gives $\langle p_t \rangle = 0.269$ GeV/c.

Imaeda[18] performed fits to the data of Bigi et al.[15] and found that the p_t distributions were well fitted by FD for baryons (T = 110-125 MeV) and PD for mesons (T = 125 MeV).

Hagedorn[22,23] has recently introduced a statistical thermodynamical model of strong interactions. He assumes that the interacting hadronic matter produced in a high energy collision can be described as an undetermined and unlimited number of hadrons in a box the size of the interaction volume. This assumption leads to the existence of a highest possible temperature to which the interaction volume approaches as the energy of the colliding particles becomes very large. The reason for the existence of a highest possible temperature can be seen as follows: in the case of classical particles where no particles can be created the temperature is proportional to E (the total system energy); for a system of photons where photons can be freely created, $T \sim E^{\frac{1}{4}}$; for the system described above all kinds of hadrons can be created so that as the system energy becomes very large it is easier to create more particles than to increase the kinetic energies of a small number of particles. Thus the temperature of the system approaches a maximum value T_o. The p_t distribution is used to determine the temperature because it is unaffected by motions along the collision axis.

In order to derive the p_t distribution Hagedorn writes down the partition function for an unlimited and undetermined number of particles in a box of volume V_o. Let $\nu_{\alpha\beta}$ be the number of particles in a given state having mass m_β and momentum p_α. A particular state is then described by listing all values of $\nu_{\alpha\beta}$, and the energy of that

state is $E_{\alpha\beta} = \sum_{\alpha,\beta} \sqrt{p_\alpha^2 + m_\beta^2}\ \nu_{\alpha\beta}$. Since we are not restricting the numbers and kinds of particles, the partition function must include contributions from all such states. Thus

$$Z(V_o,T) = \sum_{(\nu)} \exp\left[-\sum_{\alpha,\beta}\left(\frac{\sqrt{p_\alpha^2 + m_\beta^2}}{\tau}\right)\nu_{\alpha\beta}\right] \tag{17}$$

where $\sum_{(\nu)}$ goes over all possible particle configurations.

$$Z(V_o,T) = \sum_{(\nu)} \prod_{\alpha,\beta} \exp\left(\frac{-E_{\alpha\beta}\nu_{\alpha\beta}}{\tau}\right)$$

$$Z(V_o,T) = \sum_{\nu_{11}} (e^{-E_{11}/\tau\ \nu_{11}}]\ [\sum_{\nu_{12}} (e^{-E_{12}/\tau\ \nu_{12}}] \ldots.[\sum_{\nu_{\alpha\beta}} (e^{-E_{\alpha\beta}/\tau\ \nu_{\alpha\beta}}]..$$

Let $\nu_{\alpha\phi}$ refer to fermions and $\nu_{\alpha\beta}$ to bosons. Then $\nu_{\alpha\phi} = 0,1$ and $\nu_{\alpha\beta} = 0,1,2,\ldots$. Therefore

$$Z(V_o,\tau) = \prod_{\alpha,\beta} [1+e^{-E_{\alpha\beta}/\tau} + e^{-2E_{\alpha\beta}/\tau} + \ldots] \prod_{\alpha,\phi} [1+e^{-E_{\alpha\beta}/\tau}]$$

$$Z(V_o,\tau) = \prod_{\alpha,\beta} [1-e^{-E_{\alpha\beta}/\tau}]^{-1} \prod_{\alpha\phi} [1+e^{-E_{\alpha\phi}/\tau}] \tag{18}$$

Thus

$$\ln [Z(V_o,\tau)] = -\sum_{\alpha,\beta} \ln (1-e^{-E_{\alpha\beta}/\tau}) + \sum_{\alpha,\phi} \ln (1+e^{-E_{\alpha\phi}/\tau}) \ .$$

The average occupation number for the state $E_{\alpha k}$ is

$$\bar{\nu}_{\alpha k} = e^{-E_{\alpha k}/\tau} \frac{\partial}{\partial(e^{-E\alpha_k/\tau})} \ln [Z(V_0,\tau)]$$

$$\bar{\nu}_{\alpha k} = \frac{1}{e^{E_{\alpha k}/\tau}+1} \qquad \text{for fermions} \tag{19}$$

$$\text{and } \nu_{\alpha k} = \frac{1}{e^{E_{\alpha k}/\tau} - 1} \qquad \text{for bosons.} \tag{20}$$

As has already been shown, these occupation numbers lead to KD.

$$KD \equiv C\, p_t \sqrt{p_t^2+m^2}\, K_1 \left(\frac{\sqrt{p_t^2+m^2}}{\tau}\right) dp_t \tag{13}$$

For large x, $K_1(x) \approx \sqrt{\pi/2x}\ e^{-x}$. Assuming also that $p_t^2 >> m^2$ we obtain the Hagedorn distribution as

$$HD = A p_t^{3/2} e^{-p_t/\tau} . \tag{21}$$

Since HD assumes $p_t^2/m^2 >> 1$, it is expected that HD will fit pions better than nucleons.

We have fitted LD, HD, and BD to pion p_t distributions from reactions (1), (2), and (3) and to the proton p_t distribution from reaction (2)[24]. The results are shown in Table II where the χ^2 values are given per degrees of freedom. Remember that LD and HD were expected to give better results when applied to pions whereas BD should be applied to nucleons. From the values of χ^2 we find that for our data, HD gives the best fits for all cases except for pions from reaction (1) where BD provides the best fit. LD, somewhat contrary to expectations, gives a better fit to protons than to pions. The temperatures, taken from the HD fits, are 112-126 MeV for pions and 148 MeV for protons. Fits of HD, BD, and LD to pion and proton P_t distributions are shown in Figures 11 and 12. Peter Berenyi[25] has made a similar analysis of six prong $\pi^- p$ data at 7.0 GeV/c. His results are similar to ours but with a nucleon temperature significantly higher. We have analyzed

TABLE II

Results of least squares fit.

	Reaction	Type of distribution	χ^2	$c_1 \pm \Delta c_1$	$c_2 \pm \Delta c_2$
		LD	4.7	1.24 ± 0.08	170.5 ± 6.7
	1	HD	2.0	0.15 ± 0.01	126.6 ± 4.0*
		BD	0.5	0.66 ± 0.04	335.1 ±10.6
		LD	5.0	4.22 ± 0.18	145.1 ± 3.2
Pions	2	HD	1.1	0.52 ± 0.02	112.0 ± 2.1*
		BD	3.5	2.0 ± 0.08	296.7 ± 6.0
		LD	2.5	2.1 ± 0.1	163.7 ± 5.1
	3	HD	0.7	0.25 ± 0.01	122.5 ± 3.3*
		BD	2.7	1.05 ± 0.05	320.0 ± 8.5
		LD	1.7	0.44 ± 0.05	205.3 ±13.0
Proton	2	HD	0.6	0.05 ± 0.006	147.9 ± 7.5*
		BD	2.7	0.24 ± 0.02	384.7 ±19.1

*This is the value of the temperature.

$$LD = c_1 p_t \, e^{-p_t/c_2} \, dp_t$$

$$HD = c_1 p_t^{3/2} \, e^{-p_t/c_2} \, dp_t$$

$$BD = c_1 p_t \, e^{-p_t^2/c_2} \, dp_t$$

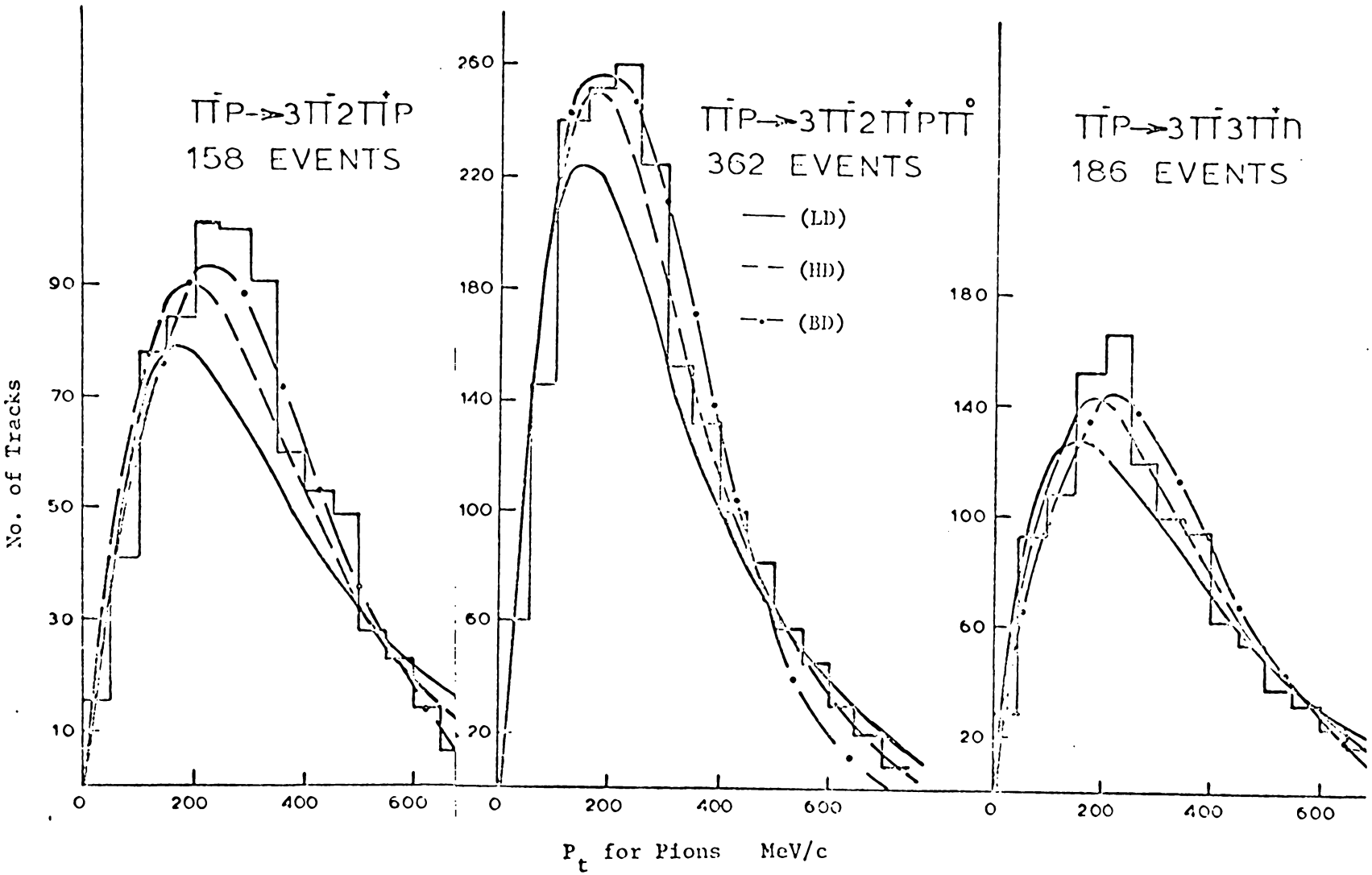

FIGURE 11. P_t Distributions for Pions from Reactions (1), (2), and (3)

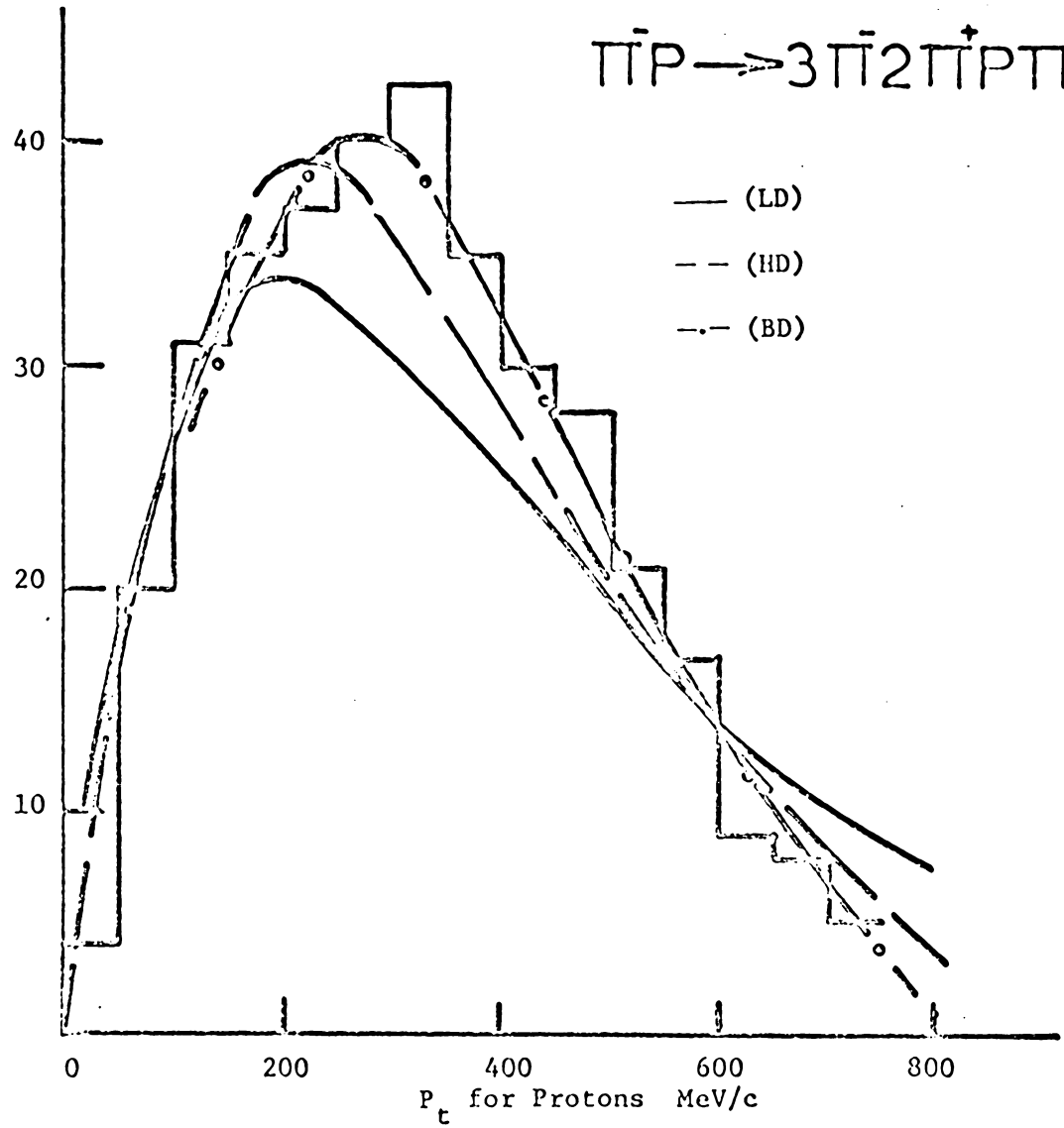

FIGURE 12. P_t Distribution for Protons from Reaction (2)

some three body final states ($\pi^- p \to \pi^- p \pi^0$, $\pi^- p \to \pi^+ \pi^- n$) and find a temperature of 150 MeV for pions.[26] This higher value is in agreement with the experimentally observed fact that T decreases with increasing multiplicity.[27]

According to Hagedorn the central regions of the interaction volume should be hotter than the outer regions. In order to examine this idea we have divided the data into two parts. The first part contains events from reactions (1) and (2) in which the proton had $-1.0 < \cos \theta_{cm} < -0.8$, and the second part is made up of events having $-0.8 < \cos \theta_{cm} < 1.0$. Hopefully the first group represents the more peripheral events and thus represents the outer regions of the interaction volume. The second group should be more representative of the center of the interacting hadronic matter. The results of fitting HD to the separated data are shown in Table III. The χ^2 values are given per degree of freedom. The temperature for peripheral events is seen to be lower than for non-peripheral events--particularly for the proton.

C. Plots of Center-of-Mass p_x Versus p_y

The distributions of the components p_x (direction of incident π^-) and p_y (arbitrary axis perpendicular to p_x) of the center of mass momenta for the particles in the reaction (2) are shown in Figure 13. The p_x and p_y (rather than p_l and p_t) representation is chosen because it displays more readily the symmetry of the center of mass distribution of particles. In simple statistical predictions p_x and p_y are equivalent. The pion plots are quite symmetrical about the origin, while

TABLE III. Fits of HD to P_t Distributions for Peripheral and Nonperipheral Events

Nature of Events	Reaction	Particle	χ^2	T ± ΔT MeV
	1	pions	2.0	130.0 ± 3.1
Peripheral	1	protons	0.9	118.0 ± 10.0
$-1.0 \leq \cos \theta_p \leq -0.8$	2	pions	0.67	105.1 ± 2.7
	2	protons	2.3	99.4 ± 8.0
	1	pions	1.2	140.3 ± 3.2
Nonperipheral	1	protons	0.3	270.0 ± 14.0
$-0.8 < \cos \theta_p \leq 1.0$	2	pions	1.6	116.9 ± 2.4
	2	protons	2.3	314.8 ± 34.0

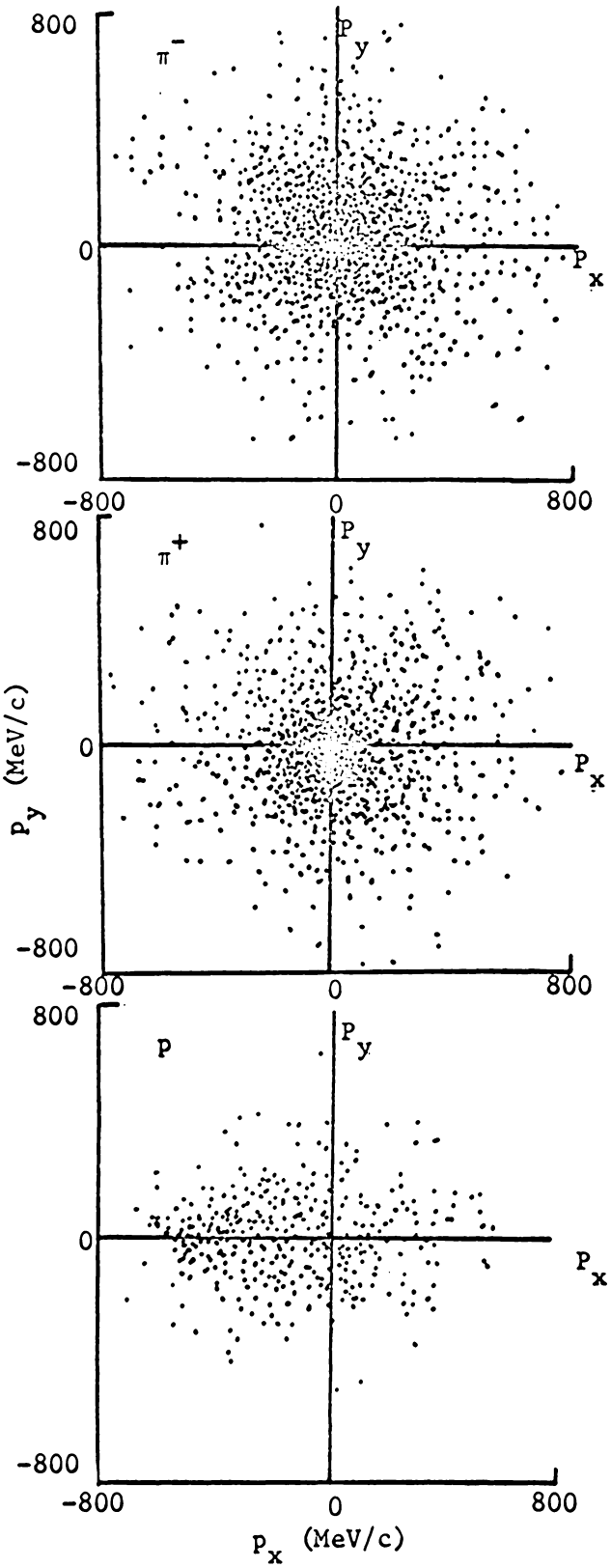

FIGURE 13. p_x Versus p_y for Pions and Protons

the proton, retaining some of its beam-like character, shows an expected shift in the backward direction. For comparison the data of Drevermann et al.[28] from four and six prong events in $\pi^+ p$ collisions at 5.0 GeV/c are shown in Figure 14.

D. Angular Correlation Between Pions

It was found in 1959 by G. Goldhaber et al.[29] in $\bar{p}p$ interactions that in the center of mass system the angles between pairs of pions differed from predictions of a simple statistical model. Specifically they found that the distribution of angles between pions of like charge differed from that of pions of unlike charge.

According to a simple statistical model the probability for $\bar{p}p$ to annihilate into N pions is given by

$$R_N = C_N P_N(\Omega)\ F_N(\omega) \tag{22}$$

where $F_N(\omega)$ is the Lorentz invariant phase space with total cm energy ω. $P_N(\Omega)$ is the probability to find N free pions in the reaction volume Ω.

$$P_N(\Omega) = \int_\Omega d^3r_1 d^3r_2 \ldots d^3r_N \left| \frac{e^{i\vec{p}_1\cdot\vec{r}_1}}{\sqrt{V}} \frac{e^{i\vec{p}_2\cdot\vec{r}_2}}{\sqrt{V}} \ldots \frac{e^{i\vec{p}_N\cdot\vec{r}_N}}{\sqrt{V}} \right|^2$$

$$P_N(\Omega) = \int_\Omega \prod_{i=1}^{N} d^3r_i \left| \frac{e^{i\sum_j p_j\cdot r_j}}{V^N} \right|^2 \tag{23}$$

V is some large normalization volume in which the single particle wave functions have periodic boundary conditions. The constant C_N is taken as

$$C_N = \text{const.}\ \frac{n(N)}{N!}$$

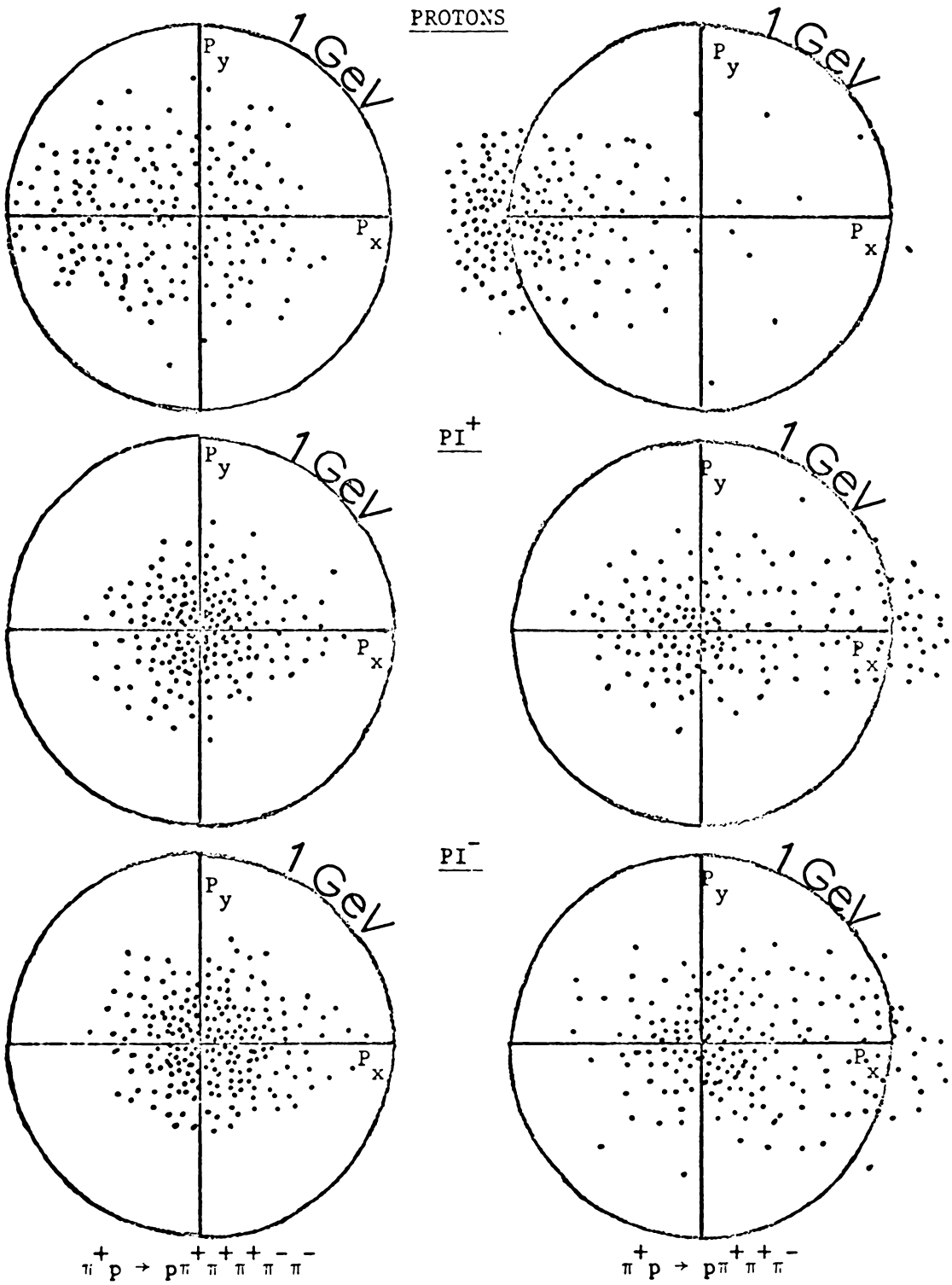

FIGURE 14. p_x Versus p_y for Pions and Protons (From Drevermann et al.[28])

where the N! implies that the particles are treated as identical and n(N) is the total number of isospin = 0,1 states (i.e. the $\bar{p}p$ initial state is a mixture of I = 0, I = 1). Thus no account is taken of the fact that pions are bosons and thus should have an overall symmetric wave function. For instance two pions in an I = 0 state must have a symmetric spatial wave function. Goldhaber et al. consider the reaction $p\bar{p} \rightarrow \pi^+\pi^+\pi^-\pi^- + n(\pi^\circ)$ where n = 0,1,2. Certainly the space part of a wave function for two pions of like charge must be symmetric. Whether the total wave function is symmetric or antisymmetric depends on I. The concession to Bose-Einstein statistics made by Goldhaber et al. is to symmetrize the wave functions of pairs of pions with like charge. For example for two positive pions the wave function is

$$\Phi(1,2) = \frac{1}{\sqrt{2V}} \{ e^{i(\vec{p}_1 \cdot \vec{r}_1 + \vec{p}_2 \cdot \vec{r}_2)} + e^{i(\vec{p}_2 \cdot \vec{r}_1 + \vec{p}_1 \cdot \vec{r}_2)} \} \qquad (24)$$

To make predictions on the angles between pion pairs, the symmetrized wave function is introduced into equation (23) and integrated over all variables except the angle between two pions. This gives $R(\phi_{12})$ (the transition rate as a function of the center of mass angle between pions 1 and 2). The predictions are expressed in terms of $\gamma = B/F$ where B is the number of pion pair angles greater than 90° and F is the number of pion pair angles less than 90°. Theoretically γ is given by

$$\gamma = \frac{\int_{-1}^{0} R_N(\cos\theta_{12})\, d(\cos\theta_{12})}{\int_{0}^{1} R_N(\cos\theta_{12})\, d(\cos\theta_{12})}$$

As an example for $p\bar{p} \rightarrow 2\pi^+2\pi^-$, the simple statistical model gives $\gamma = 2.2$. This is physically reasonable since momentum must be conserved and the four pions have available to them a solid angle of 4π. The average angle will certainly be greater than 90°.

The value of γ depends sensitively on ρ (the radius of the interaction volume) as might be expected from equation (23). Some computed values of γ for like and unlike pions from $p\bar{p} \rightarrow 2\pi^+2\pi^- + n(\pi^\circ)$ (n = 0,1,2) are given in Table IV. The interaction radius ρ is expressed in terms of pion Compton wave lengths. For all listed values of ρ, γ for unlike pions is greater than γ for like pions. Our data show good qualitative agreement with this theory as is seen in Table V. The only disagreement is $\gamma(\pi^-\pi^-)$ from reaction (1) which is larger than $\gamma(\pi^+\pi^-)$ and $\gamma(\pi^+\pi^+)$ for this reaction. Note that our values are smaller than those in Table V. This is due to the fact that our final states have higher multiplicities so that the average angles between pairs of particles is smaller.

TABLE IV

Some Computed Values of the Angular Correlation Parameter $\gamma=B/F$ for Various Values of the Interaction Volume Radius ρ.

ρ	γ (like)	γ (unlike)
0.3	1.57	1.91
0.5	1.41	1.95
0.75	1.38	1.91
1.0	1.44	1.87
2.0	1.66	1.79

TABLE V

Values of the Angular Correlation Parameter $\gamma=B/F$

Reaction	$\pi^+\pi^+$	$\pi^-\pi^-$	$\pi^+\pi^-$
1	1.20 ± .21	1.45 ± .18	1.20 ± .12
2	1.19 ± .18	1.27 ± .10	1.36 ± .08
3	1.25 ± .15	1.18 ± .14	1.39 ± .09

SECTION V

ANGULAR DISTRIBUTIONS AND RESONANCE PRODUCTION

A. Angular Distributions

Figures 15 through 17 show the center of mass angular distributions for final state particles from reactions (1), (2), and (3). The charged pions are peaked slightly forward in reactions (1) and (2). The neutral pions in reaction (2) are practically isotropic. The protons in reactions (1) and (2) are peaked strongly backward. In reaction (3) the charged pions are again nearly isotropic with a slight forward peaking. The negative pions show considerably less forward peaking in reaction (3) than in reactions (1) and (2) due to the lack of a beam-like pion. The neutrons in reaction (3) are peaked backward.

To illustrate the assymetries in six prong interactions we have calculated the assymetry parameter $\alpha \equiv \frac{F-B}{F+B}$. Here F represents particles with center of mass production angles $\leq 90°$ and B represents angles $> 90°$ and $\leq 180°$. Table VI shows the results of our data from reactions (1), (2), and (3). It is found that α shows a definite dependence on incident momentum. Figure 18 shows the dependence of α on the momentum of the incident pion for the reaction $\pi^- p \rightarrow \pi^- \pi^- \pi^- \pi^+ \pi^+ p$. The data is taken from experiments at 5.5[30], 7.0[24,25], 8.5[31,32], 10.0[33], and 16[34] GeV/c. Although α for positive pions doesn't show much variation, the protons are seen to move more backward while the negative pions go more forward with increasing incident momentum. This implies that some peripheral behavior is still present in these high multiplicity events.

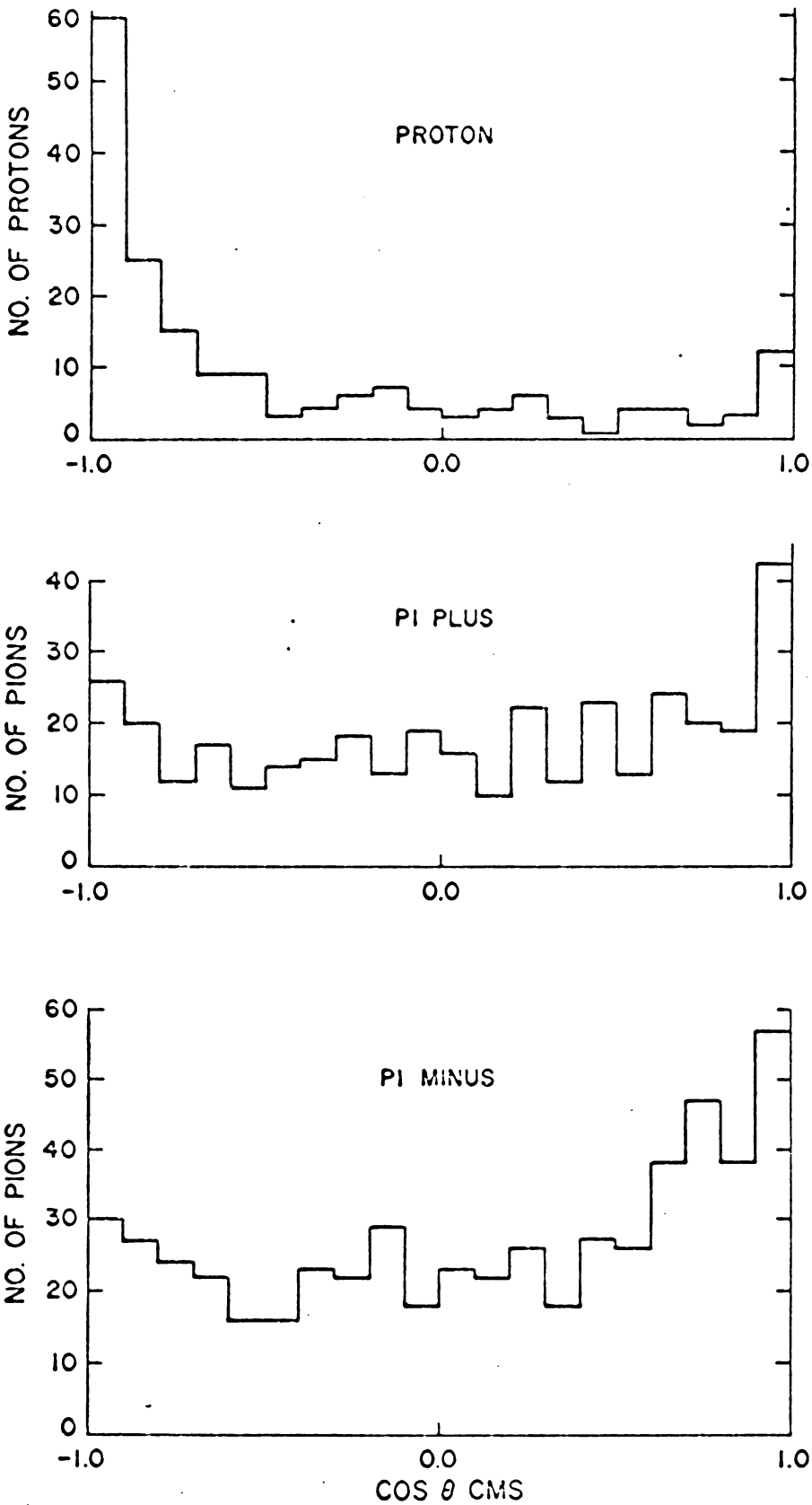

FIGURE 15. CMS Angular Distributions from Reaction (1).

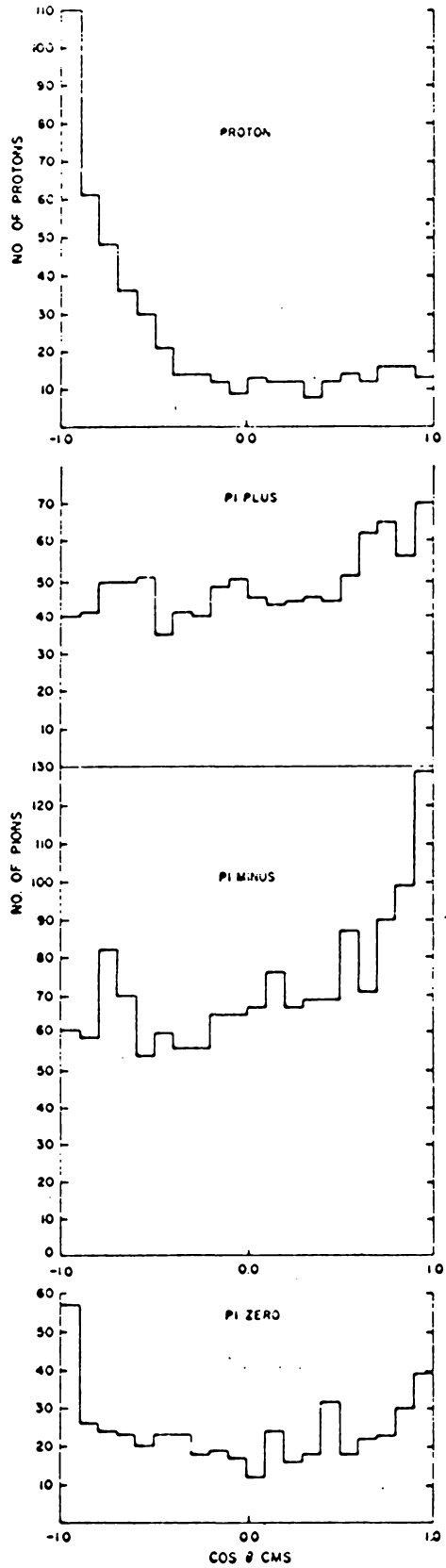

FIGURE 16. CMS Angular Distributions from Reaction (2).

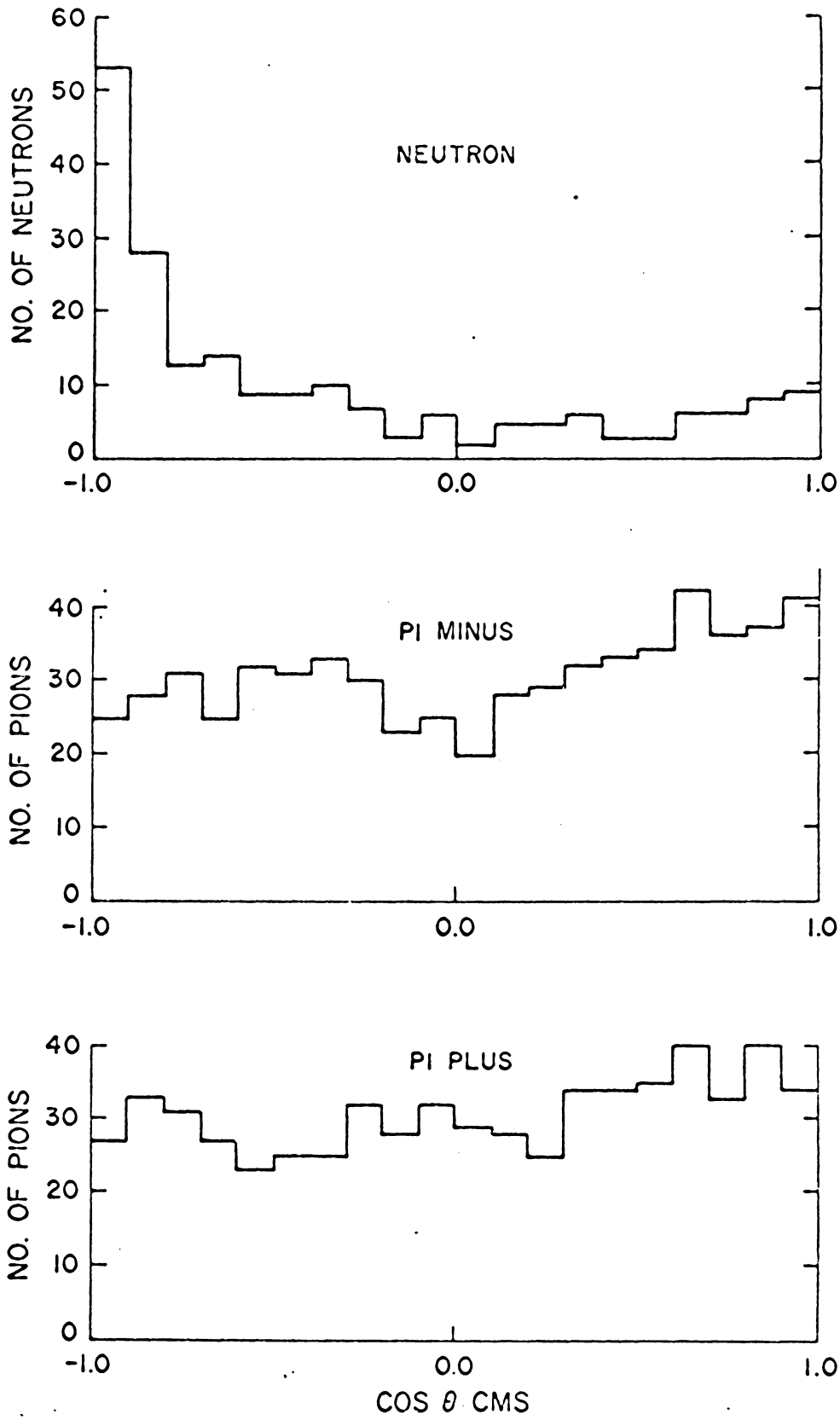

FIGURE 17. CMS Angular Distributions from Reaction (3).

TABLE VI

Values of the Assymetry Parameter

Reaction	Nucleon	π^+	π^-	π^0
1	-0.55 ± .07	0.10 ± .05	0.16 ± .04	
2	-0.42 ± .03	0.09 ± .03	0.07 ± .02	0.02 ± .01
3	-0.50 ± .06	0.15 ± .04	0.10 ± .04	

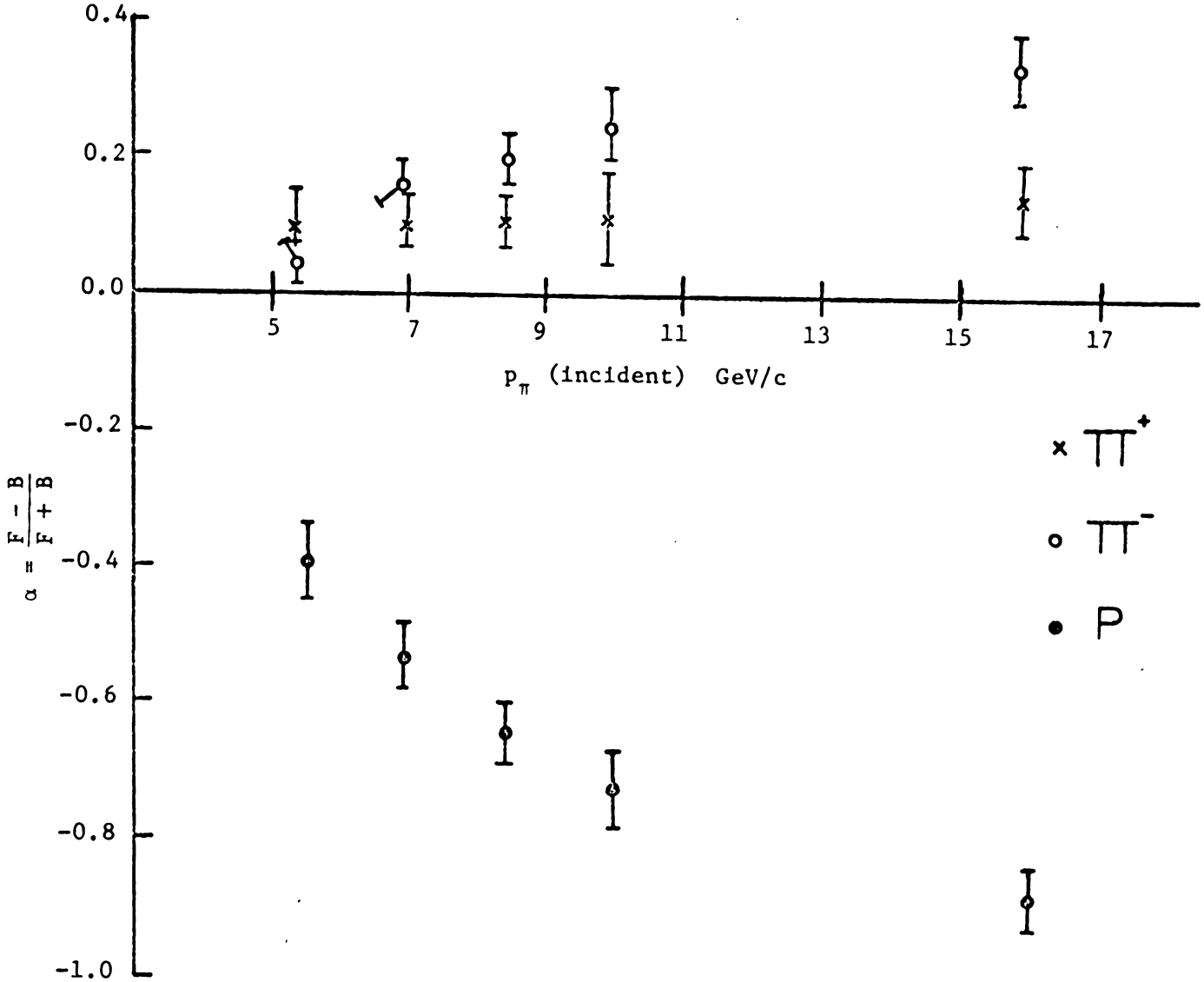

FIGURE 18. Variation of the Assymetry Parameter with Incident Momentum

B. Resonance Production

Whether a resonance is a short-lived bound state of two or more particles or a particle which rapidly decays into two or more particles is not known and perhaps is not relevant. What is relevant is that a resonance can be assigned quantum numbers such as spin, parity, strangeness, baryon number etc. Because they are very short lived ($\simeq 10^{-23}$ seconds) there is an uncertainty in the mass of a resonance so that resonances are assigned a central mass and a width.

The most common way to search for resonance production in high energy bubble chamber experiments is to study effective mass distributions. A resonance decaying into a particular combination of particles will appear as a bump in the effective mass distribution for that combination of particles.

In order to analyze the masses and widths of resonances one usually assumes that, given a final state of N particles, the probability to produce a subset of K particles having total energy ω in their center of mass is

$$F(\omega)\, d\omega = PS(\omega)\, [A + B\, \frac{\Gamma_1^2}{(\omega-\omega_2^0)^2 + \frac{\Gamma_1^2}{4}} + C\, \frac{\Gamma_2^2}{(\omega-\omega_2^0)^2 + \frac{\Gamma_2^2}{4}} + \ldots] \quad (26)$$

PS represents the distribution which would result if the interaction matrix element were constant (ie. the distribution predicted by phase space. See Equation 4). The matrix element contribution has been expanded as a constant plus a sum of Breit-Wigner (BW) resonance forms. Thus Γ_i represents the width and ω_i^0 the central mass of resonance i. Then given the effective mass distribution for a particular combination

of particles Equation (26), with the proper phase space background and number of BW's, can be fitted to the distribution. In this way the masses and widths of resonances can be determined. Before Equation (26) can be used, however, it is necessary to calculate the phase space background (PS). From Equation (5) N-body phase space is

$$R_N(p,E) = \int [\prod_{i=1}^{N} d^4q_i \quad (q_i^2 - m_i^2)] \; \delta^4(\sum_{j=1}^{N} q_j - Q) \tag{5}$$

One is interested in the variation of R_N as a function of the effective mass of a subset of k particles. Thus it is necessary to calculate

$$PS(m) = \frac{dR_N(p,E)}{d(M_N^k)^2} = \int \prod_{i=1}^{N} d^4q_i \delta(q_i^2 - m_i^2)] \delta^4(\sum_{j=1}^{N} q_i - Q) \delta(m^2 - (M_N^k)^2)$$

where M_N^k is the four momentum of the center of mass of k particles in an N body final state. Now

$$\int \delta^4(\sum_{i=1}^{k} q_i - M_N^k) \; d^4M_N^k = 1$$

and $$\delta^4(\sum_{i=1}^{N} q_i - Q) = \int \delta^4(\sum_{i=1}^{k} q_i - M_N^k) \delta^4(M_N^k + \sum_{i=k+1}^{N} q_i - Q) d^4M_N^k.$$

Thus

$$PS(m) = \int [\prod_{i=1}^{N} d^4q_i \delta(q_i^2 - m_i^2)] \delta(m^2 - (M_N^k)^2) \delta^4(\sum_{i=1}^{k} q_i - M_N^k)$$

$$\times \delta^4(M_N^k + \sum_{i=k+1}^{N} q_i - Q) \; d^4M_N^k$$

$$PS(m) = \int \{ [\prod_{i=1}^{k} d^4q_i \delta(q_i^2 - m_i^2) \delta^4(\sum_{j=1}^{k} q_i - M_N^k)]$$

$$\times [\prod_{i=k+1}^{N} d^4q_i \delta(q_i^2 - m_i^2) d^4M_N^k \; \delta(m^2 - (M_N^k)^2 \delta^4(\sum_{j=k+1}^{N} q_j + M_N^k - Q)] \}$$

The first term in brackets is seen to be the Lorentz invariant phase of k particles with total four momentum M_N^k. The second term in brackets is the Lorentz invariant phase space of N-k+1 particles (N-k from the N body final state and the extra particle having mass m and four momentum M_N^k). Expressing the first term in the center of mass of the k particles and the second in the overall center of mass the result is

$$PS(m) = R_k(o,m,m_1,m_2,\ldots,M_k)\ R_{N-k+1}(o,E,M_{k+1},\ldots,M_N,M) \qquad (27)$$

Hereafter Equation (26) with n Breit-Wigner resonance forms will be referred to as PS plus n-BW's.

1. Reaction (1)

In Figure 19 is shown the $p\pi^+$ and $\pi^+\pi^-$ effective mass distributions. A PS plus BW fit to the $p\pi^+$ mass distribution gives for the $\Delta^{++}(1238)$ a mass of 1190 ± 30 MeV/c^2 with a width of 80 ± 30 MeV/c^2. for the ρ (760) in the $\pi^+\pi^-$ mass plot a fit of PS plus BW gives $M(\rho)$ = 750 ± 20 MeV/c^2 and $\Gamma(\rho)$ = 105 ± 35 MeV/c^2. The cross sections for Δ^{++} (1238) and $\rho(760)$ in this channel are estimated to be 50 ± 20 μb and 120 ± 30 μb. The explanation for the low value of mass for Δ^{++} (1238) is found in a paper by J. D. Jackson[35]. According to Jackson, if $d\sigma_s(\omega)$ is the cross section for the production of a stable particle R_o of mass ω then the cross section to produce a resonance which then decays is

$$d\sigma = d\sigma_s(\omega) = \left[\frac{\omega_o/\pi\ \Gamma(\omega)}{(\omega_o^2-\omega^2)+\omega_o^2\Gamma^2(\omega)}\right] d\omega^2$$

where $\Gamma(\omega)$ is the width and ω_0 the mass of the resonance. If the decay is into two bodies with relative orbital angular momentum ℓ, then $\Gamma \simeq \Gamma_0 \left(\frac{q}{q_0}\right)^{2\ell+1}$ where $\Gamma_0 = \Gamma(\omega_0)$, q is the momentum of one of the decay products in the resonance's rest frame, and q_0 is the total energy in that frame. In this approximation Jackson finds that the resonance peak is shifted by an amount

$$\frac{\omega_0 - \omega_{peak}}{\Gamma_0} \simeq \frac{2\ell+1}{8} \left(\frac{\Gamma_0}{\omega_0}\right) \left[\frac{\omega_0^4 - (m_1^2 - m_2^2)^2}{\omega_0^4 - 2(m_1^2+m_2^2)\omega_0^2 + (m_1^2 - m_2^2)}\right] \qquad (29)$$

For the Δ^{++} (1238), assuming $\Gamma_0 = 125$ MeV/c^2, this gives a shift of approximately 23 MeV/c^2 causing the peak to occur at about 1215 MeV/c^2.

In order to search for 'A' mesons we have chosen events having a $\pi^+\pi^-$ mass combination in the $\rho(760)$ band (650-850 MeV/c^2) and plotted $\rho\pi$ mass distributions. The $\rho\pi^+$ and $\rho\pi^-$ mass plots are shown in Figures 20-a and 20-b. There is no evidence for 'A' meson production.

2. Reaction (2)

In Figure 21 is plotted the $\pi^+\pi^-\pi^0$ mass distribution. From the rather broad hump in the ω region we estimate our mass resolution to be approximately 30 MeV/c^2. The $p\pi^+$, $p\pi^-$, and $p\pi^0$ mass distributions are shown in Figure 22. The $p\pi^+$ mass plot shows considerable production of Δ^{++} (1238). A fit of PS plus BW to the $p\pi^+$ mass distribution gives 1180 ± 30 MeV/c^2 for the Δ^{++} (1238) mass. The width is 110 ± 30 MeV/c^2 and the cross section for Δ^{++} (1238) production in this channel is estimated to be 150 ± 30 μb. The $p\pi^0$ mass distribution shows an enhancement at 1540 ± 20 MeV/c^2 with

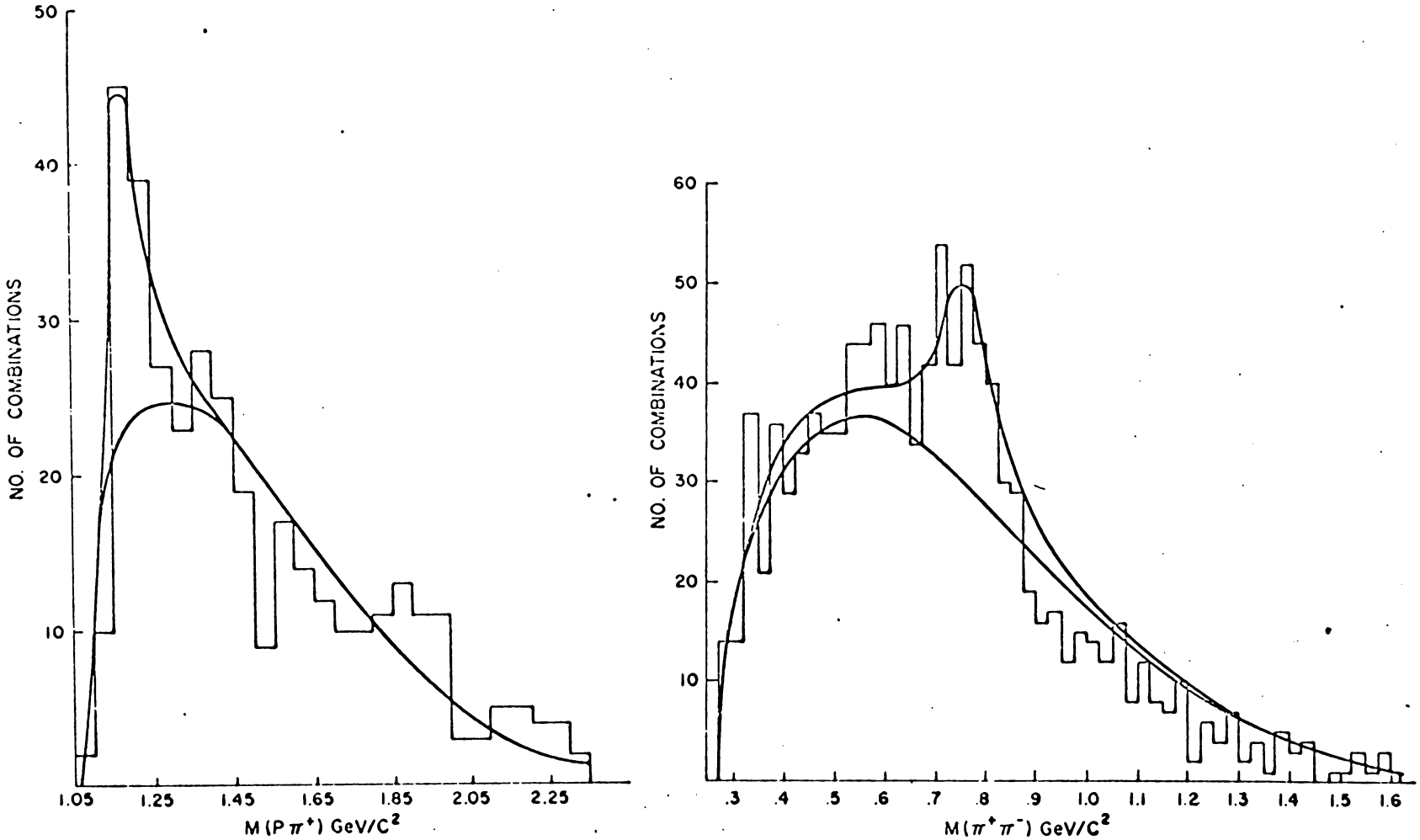

FIGURE 19. $p\pi^+$ and $\pi^+\pi^-$ Effective Mass Distributions

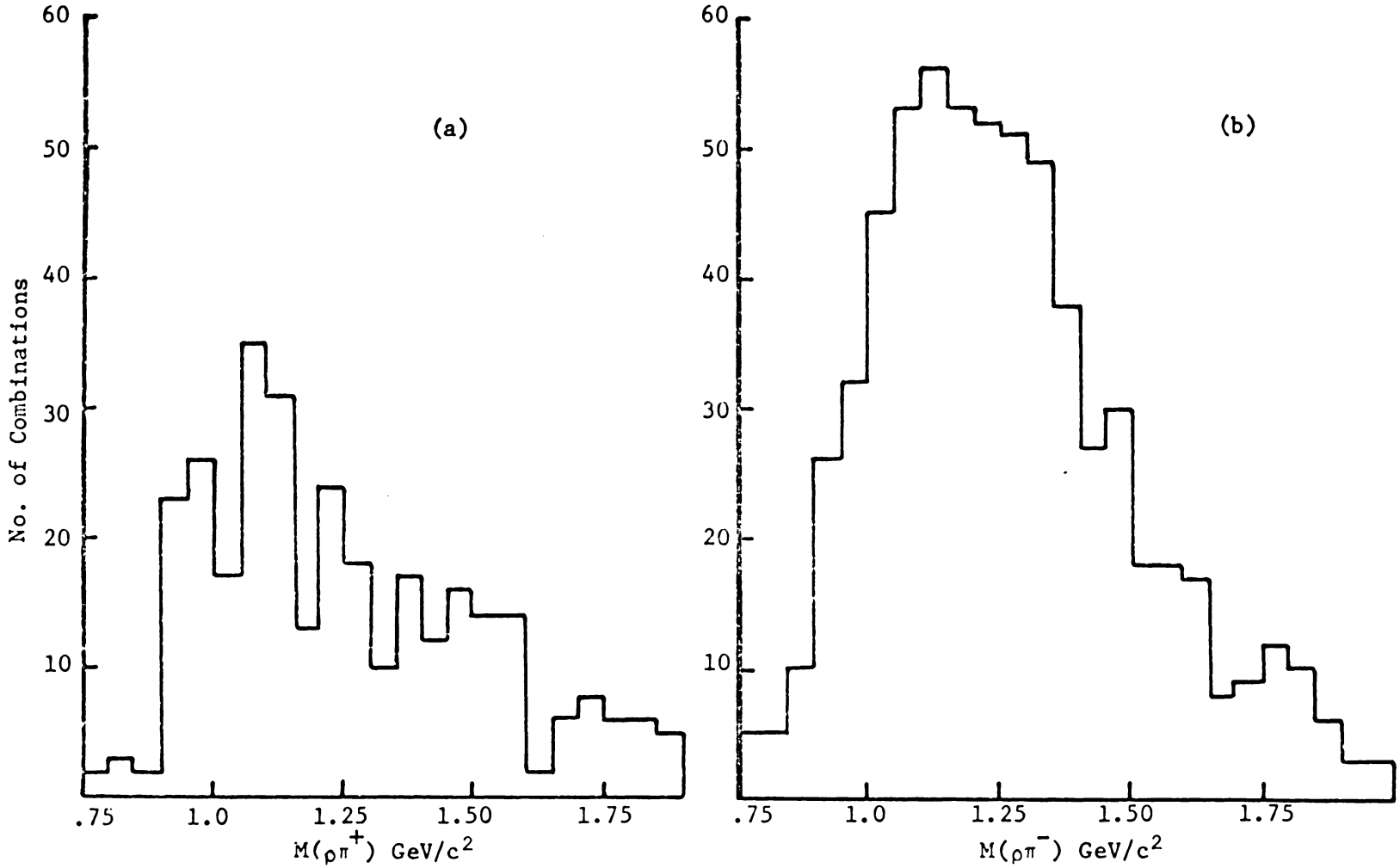

FIGURE 20. $\rho\pi^+$ and $\rho\pi^-$ Effective Mass Distributions

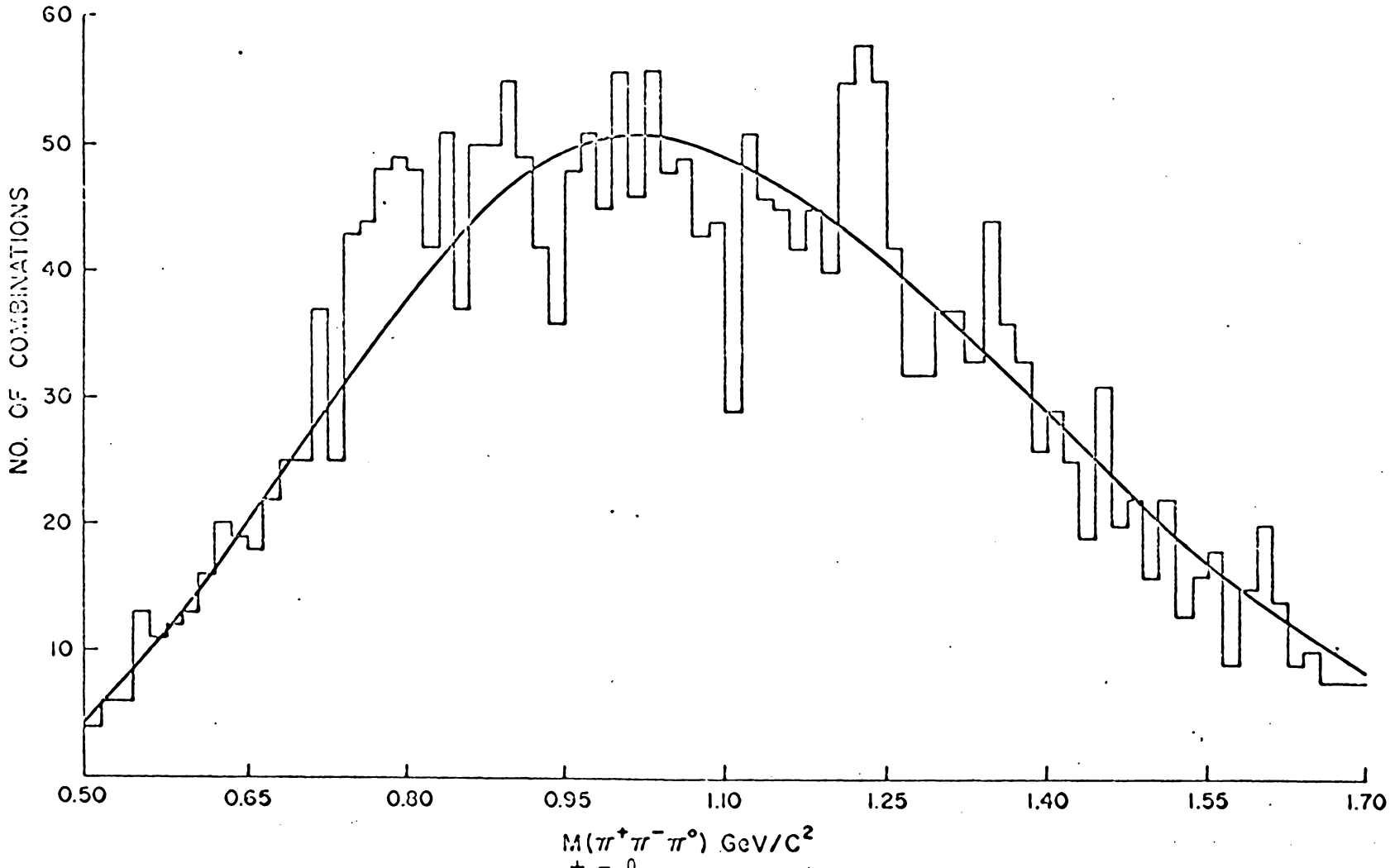

FIGURE 21. $\pi^+\pi^-\pi^0$ Effective Mass Distributions

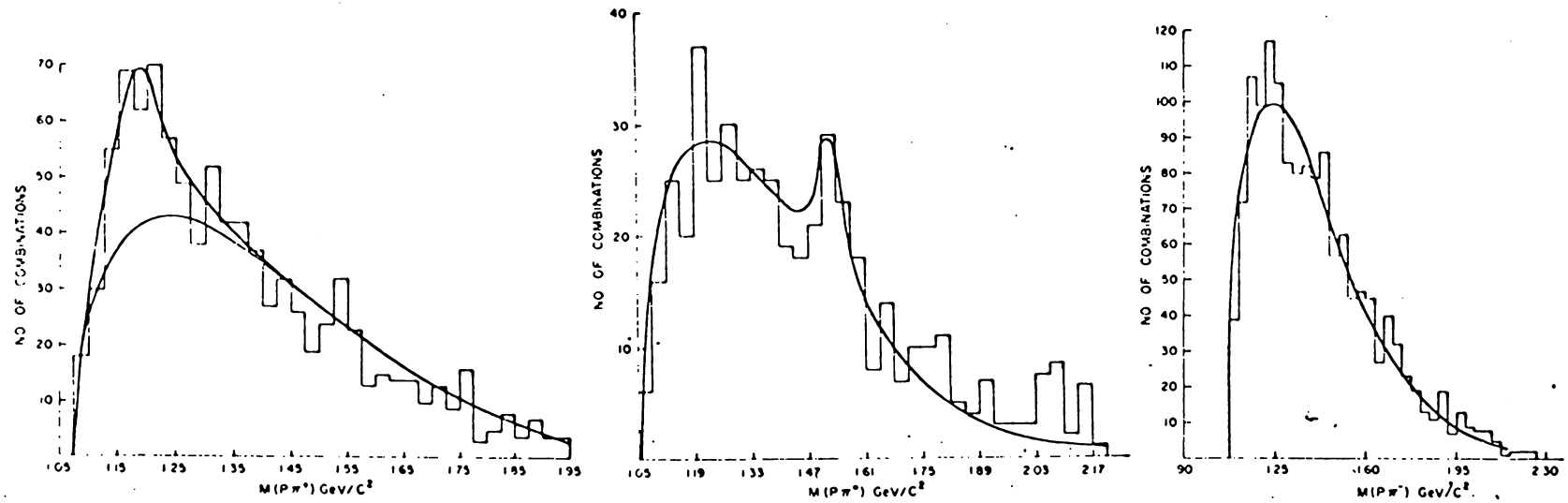

FIGURE 22. $p\pi^+$, $p\pi^0$, and $p\pi^-$ Effective Mass Distributions from Reaction (2)

width 100 ± 40 MeV/c^2. This is interpreted as $N^*(1520)$ and the cross section in 40 ± 10 μb. The $p\pi^-$ mass plot is shown with 100% PS normalization. In order to look for R, S, and T mesons we have plotted $\pi^+\pi^+\pi^-\pi^-\pi^0$ mass combinations in Figure 23. No significant enhancements are observed.

In Figure 24-a is shown the $\pi^+\pi^-\pi^+\pi^-$ mass plot. A fit of PS plus two BW's gives for the two peaks masses of 1085 ± 20 MeV/c^2 and 1470 ± 20 MeV/c^2 with widths 70 ± 30 MeV/c^2 and 60 ± 25 MeV/c^2. These peaks are about 3 standard deviation effects. Since resonances have not been observed at these energies in the $(4\pi)^0$ channel before we have attempted to study the nature of these peaks. As there are only two positive pions in this final state the first attempt to study these peaks was to remove events having a $p\pi^+$ mass combination in the $\Delta^{++}(1238)$ band (1120-1340 MeV/c^2). The results of this removal are that the peaks disappear indicating that they are probably not resonances but enhancements associated with $\Delta^{++}(1238)$ production (Figure 24-b). To support this belief Figure 25 shows the $\pi^+\pi^-\pi^+\pi^-$ mass plot for events in the $\Delta^{++}(1238)$ band. The two peaks are very prominent. Finally Figure 26 shows a scatter plot of $M(p\pi^+)$ versus $M(\pi^+\pi^-\pi^+\pi^-)$. The plot again shows that the contribution to the two $(4\pi)^0$ peaks comes from the $\Delta^{++}(1238)$ band.

3. Reaction (3)

Figure 27 shows the $N\pi^+$ and $N\pi^-$ mass plots. Both are shown with 100% PS normalization. The $\pi^+\pi^-\pi^+\pi^-$ mass distribution (Figure 28) again shows two peaks which are about 2.5 standard deviation effects.

The masses are 1075 ± 20 MeV/c^2 and 1495 ± 25 MeV/c^2, and the widths are 60 ± 30 MeV/c^2 and 50 ± 30 MeV/c^2. The $(4\pi)^0$ mass distribution was plotted for events having no $N\pi^-$ mass combination between 1120 and 1340 MeV/c^2. The results were inconclusive because of the small number of events which remained.

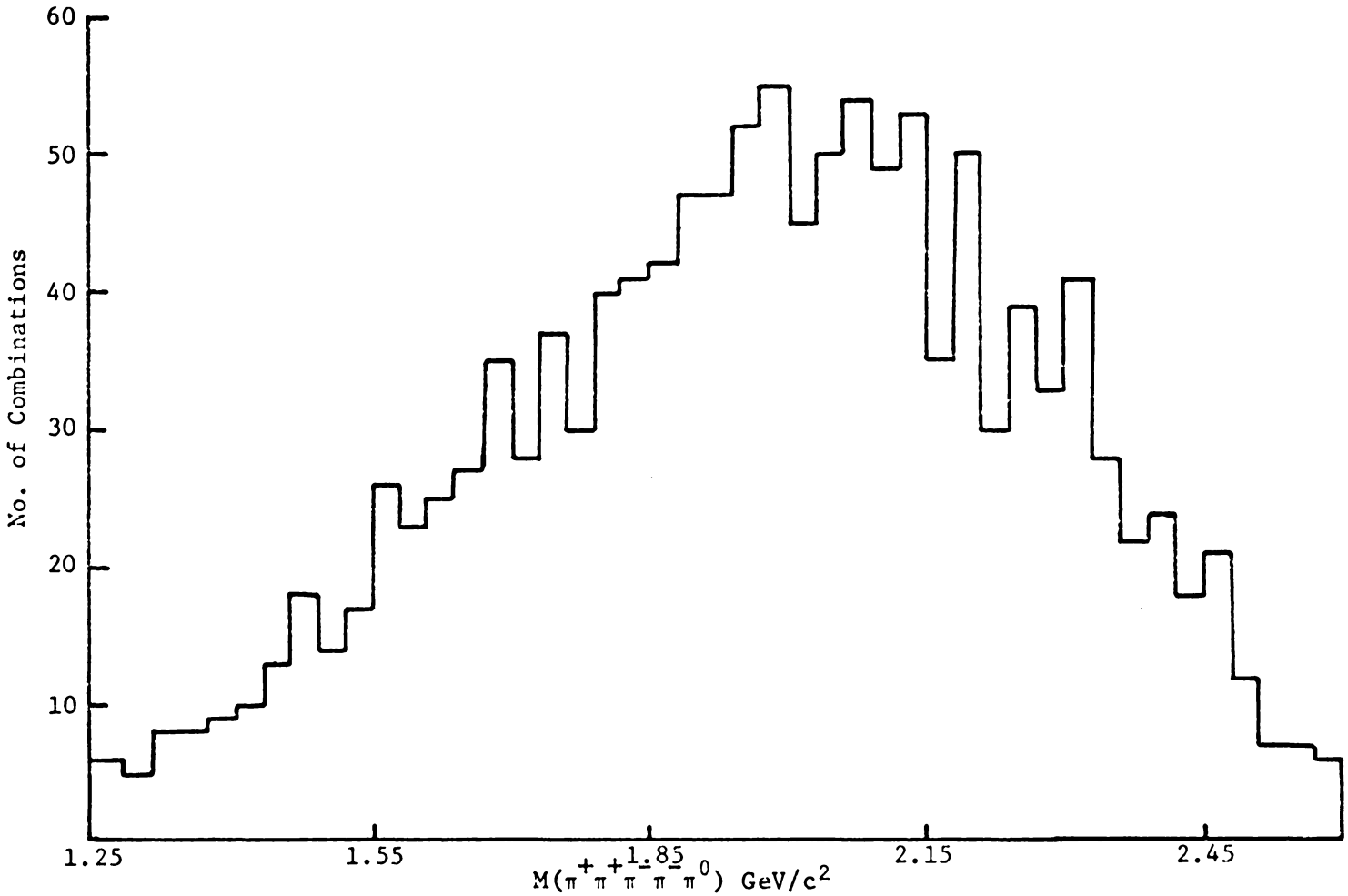

FIGURE 23. Effective Mass Distribution for $\pi^+\pi^+\pi^-\pi^-\pi^0$ from Reaction (2).

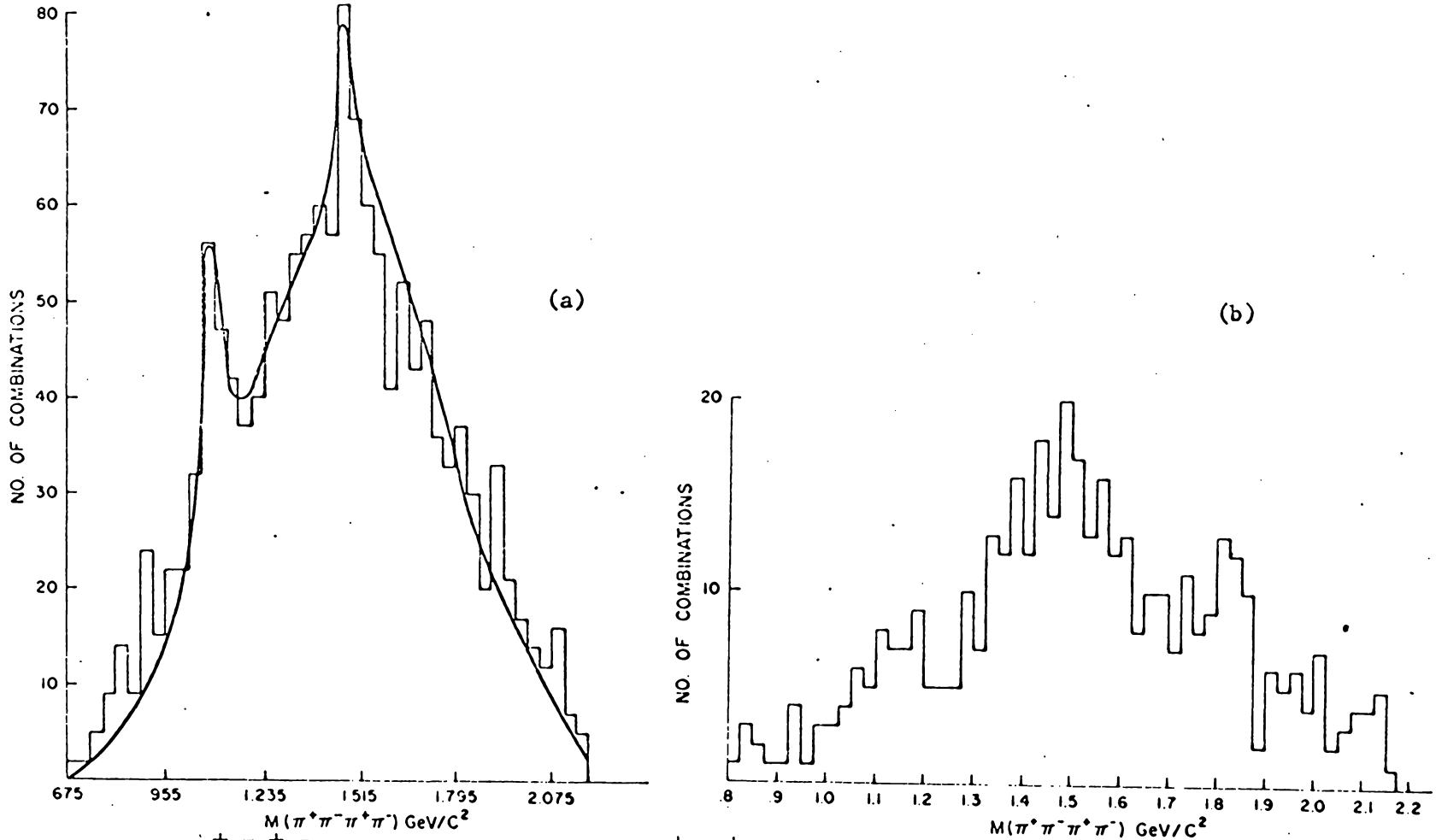

FIGURE 24. (a) $\pi^+\pi^-\pi^+\pi^-$ Mass Distribution. (b) $\pi^+\pi^-\pi^+\pi^-$ Mass Distribution Omitting Events in $\Delta^{++}(1238)$ Band.

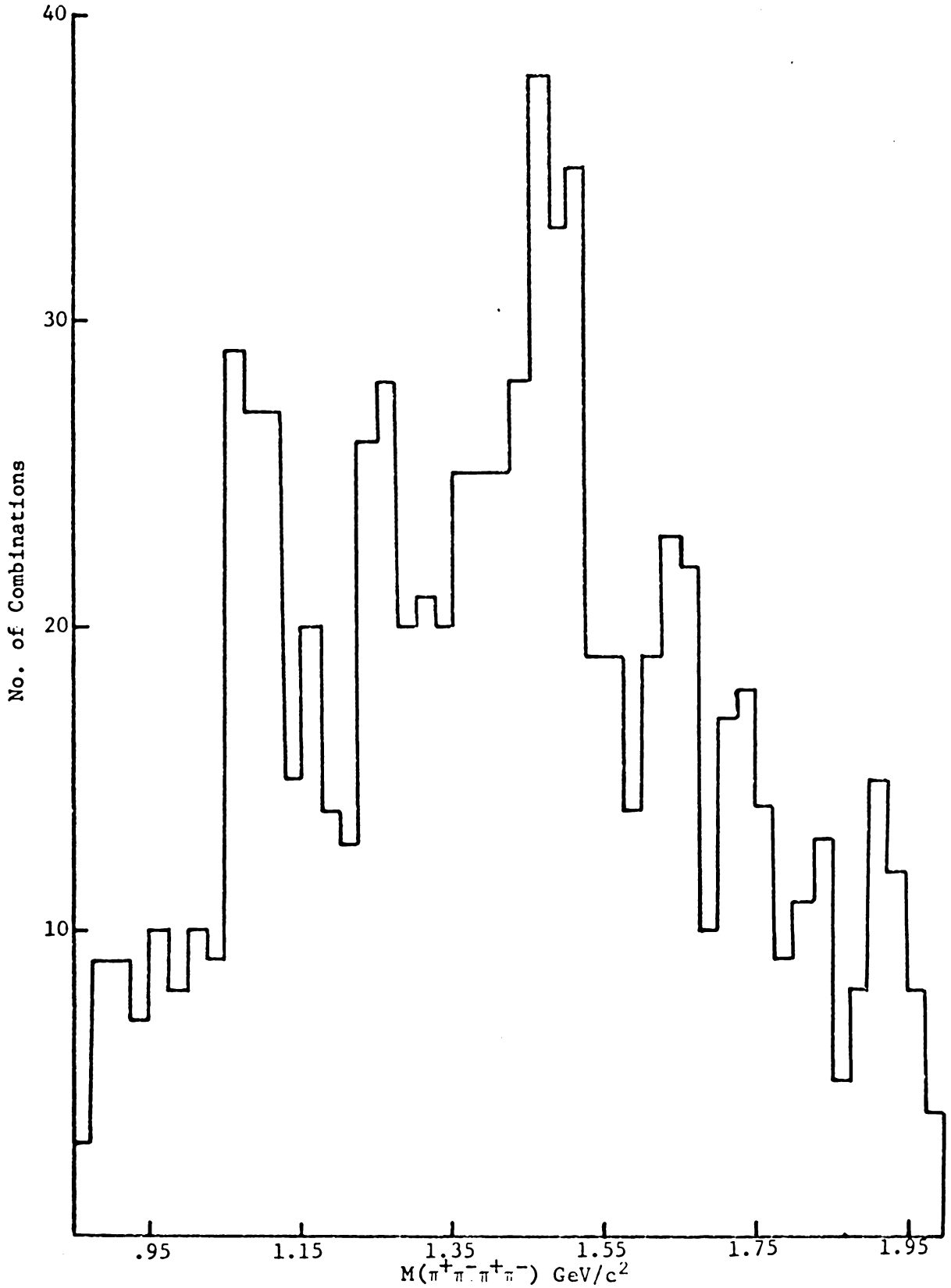

FIGURE 25. $\pi^+\pi^-\pi^+\pi^-$ Mass Distribution for Events in the $\Delta^{++}(1238)$ Band.

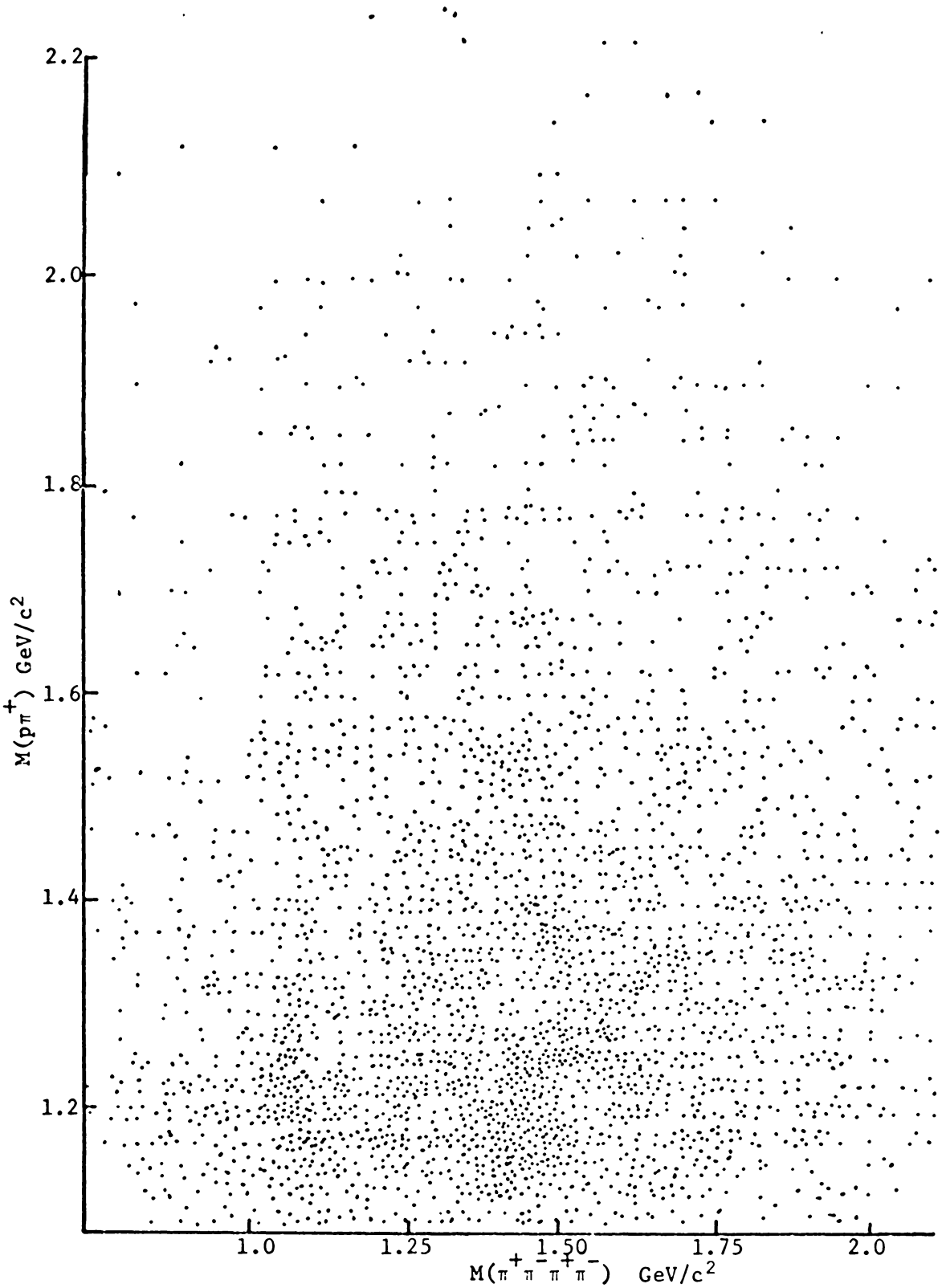

FIGURE 26. $M(p\pi^+)$ Versus $M(\pi^+\pi^-\pi^+\pi^-)$ for Reaction (2).

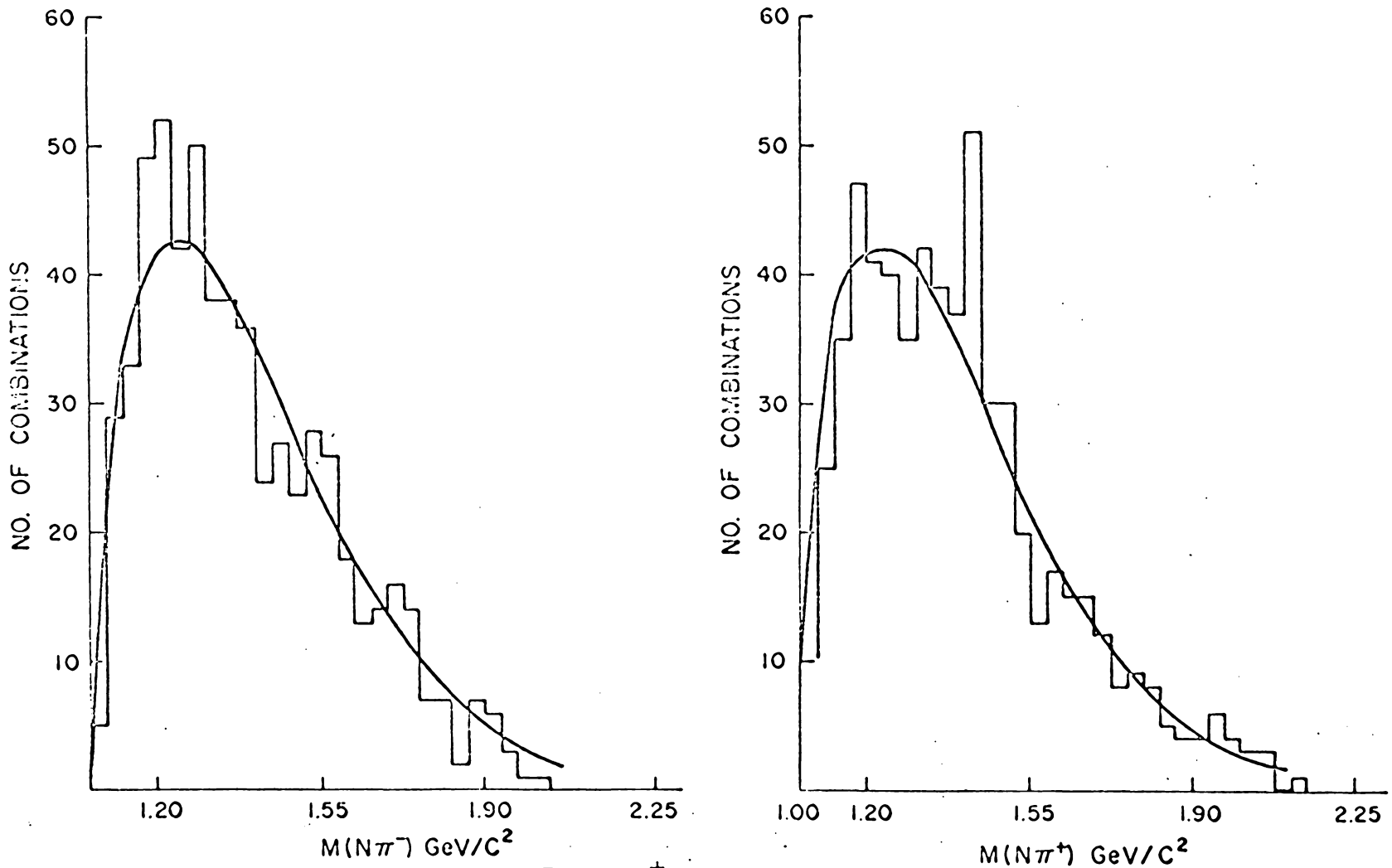

FIGURE 27. $N\pi^-$ and $N\pi^+$ Effective Mass Distributions.

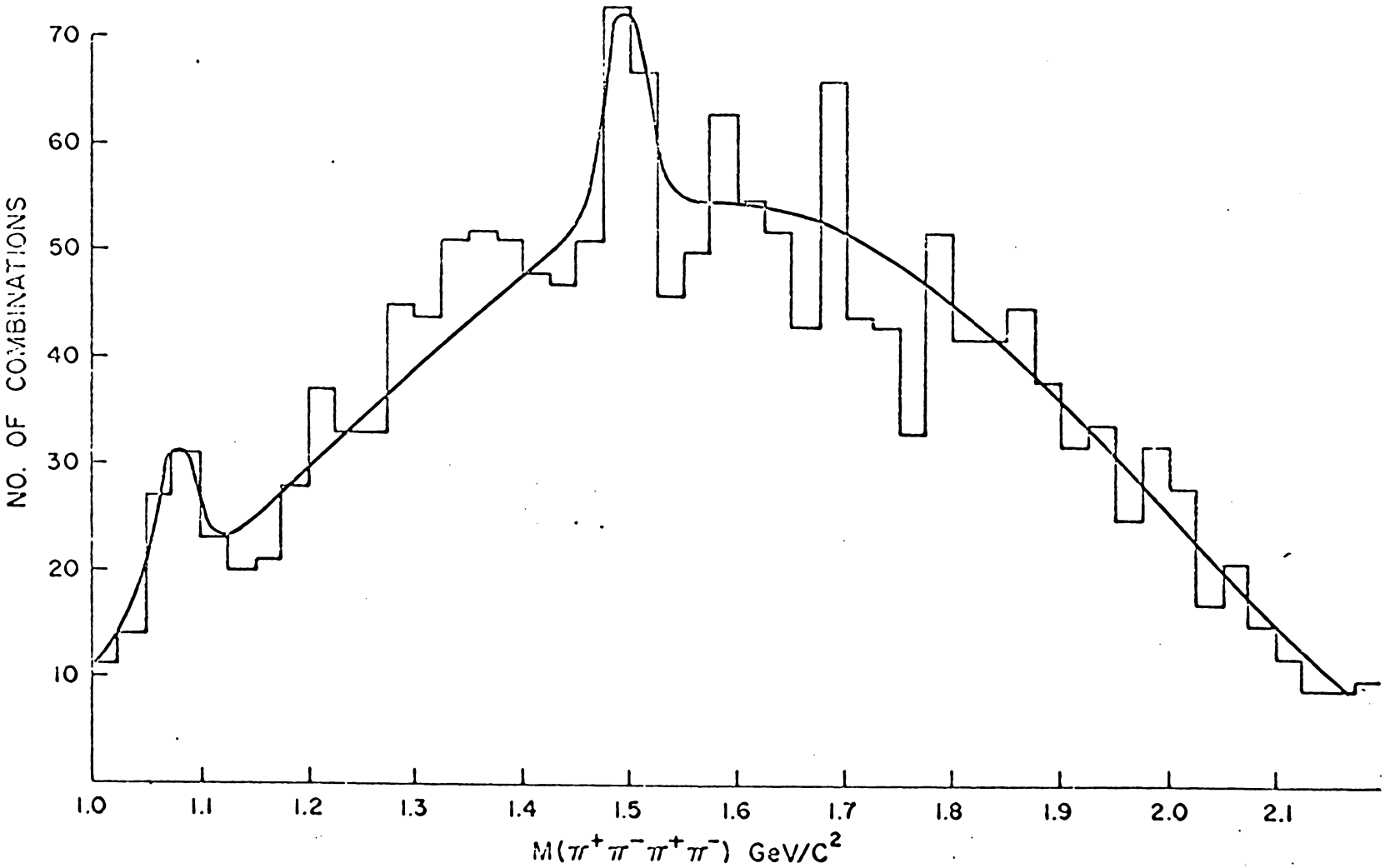

FIGURE 28. $\pi^+\pi^-\pi^+\pi^-$ Mass Distribution from Reaction (3).

SECTION VI

SUMMARY AND CONCLUSIONS

We have measured six prong events from a $\pi^- p$ experiment at 7.0 GeV/c. The total cross section is 2.40 ± 0.27 mb and the partial cross sections are: (1) $\pi^- p \rightarrow \pi^- \pi^- \pi^- \pi^+ \pi^+ p$ - 0.22 ± 0.04 mb, (2) $\pi^- p \rightarrow \pi^- \pi^- \pi^- \pi^+ \pi^+ p\pi^0$ - 0.58 ± 0.09 mb, and (3) $\pi^- p \rightarrow \pi^- \pi^- \pi^- \pi^+ \pi^+ \pi^+ n$ - 0.24 ± 0.05 mb. The center of mass momentum spectra for particles produced in the six prong interactions are in fair agreement with phase space predictions. We have fitted transverse momentum spectra to linear distribution (LD), Hagedorn distribution (HD), and Boltzmann distribution (BD). HD provides the best fit for all cases except for pions in reaction (1) where BD gives the best fit. One of the parameters in the Hagedorn distribution is the temperature of the interaction volume. The value of the temperature obtained from the pion spectra is 112-126 MeV, and from the proton p_t spectrum it is 148 MeV.

The center of mass angular distributions for pions and nucleons are shown. The nucleons show some backward peaking. A group of negative pions travels in the most forward direction. The pions produced in the interaction show fairly isotropic angular distributions. The measured value of the assymetry parameter $\alpha = \frac{F-B}{F+B}$ indicates some peripheralism.

We have measured angles between pairs of pions in the center of mass. Our data shows that the angles between pions of the same charge are on the average smaller than the angles between pairs of pions of

opposite charge, which is in agreement with Goldhaber's predictions.

We have investigated the effective mass distributions of various combinations of particles in reactions (1), (2), and (3). In reaction (1) we find Δ^{++} (1238) and ρ(760) with production cross sections 50 ± 20 μb and 120 ± 30 μb.

The mass and width of the Δ^{++} (1238) are found to be 1190 ± 30 MeV/c^2 and 80 ± 30 MeV/c^2. For the ρ(760) the mass and width are 750 ± 20 MeV/c^2 and 105 ± 35 MeV/c^2. In reaction (2) we find Δ^{++} (1238) with mass 1180 ± 30 MeV/c^2 and width 110 ± 30 MeV/c^2. The cross section for Δ^{++} (1238) production in reaction (2) is 150 ± 30 μb. There is an enhancement in the $p\pi^0$ mass distribution at 1540 ± 20 MeV/c^2 with width 100 ± 40 MeV/c^2. This is interpreted as N* (1520) and the cross section is 40 ± 10 μb. In the $\pi^+\pi^-\pi^+\pi^-$ mass distribution we find peaks at 1085 ± 20 MeV/c^2 and 1470 ± 20 MeV/c^2. Both peaks represent three standard deviation effects. Their widths are 70 ± 30 MeV/c^2 and 60 ± 25 MeV/c^2. To investigate these peaks we plotted the $(4\pi)^0$ mass distribution for events having no $p\pi^+$ mass combination in the Δ^{++} (1238) band (1120-1340 MeV/c^2). The two peaks disappeared indicating that they are probably not resonances but enhancements associated with Δ^{++} (1238). In the $\pi^+\pi^-\pi^+\pi^-$ mass distribution from reaction (3) there are peaks at 1075 ± 20 MeV/c^2 and 1495 ± 25 MeV/c^2 which are about 2.5 standard deviation effects. The widths of these peaks are 60 ± 30 MeV/c^2 and 50 ± 30 MeV/c^2. A removal of events having an $N\pi^-$ mass combination between 1120 and 1340 MeV/c^2 was inconclusive because of the small number of remaining events.

REFERENCES

1. M. N. Focacci et al., Phys. Rev. Letters 17, 890 (1966).
2. A. Bettini et al., Nuovo Cimento 42A, 695 (1966).
3. N. N. Biswas et al., Phys. Rev. Letters 21, 50 (1968).
4. J. A. Danysz et al., Nuovo Cimento 51A, 801 (1967).
5. G. Ascoli et al., Phys. Rev. Letters 21, 113 (1968).
6. J. W. Lamsa et al., Phys. Rev. 166, 1395 (1968).
7. M. Abolins et al., Phys. Rev. Letters 11, 381 (1963).
8. C. Baltay et al., Phys. Rev. Letters 18, 93 (1967).
9. Bartsch et al., Phys. Letters 11, 167 (1964).
10. W. P. Trower, Ph.D. Thesis, Univ. of Illinois (1966).
11. S. H. Chin, M. S. Thesis, Ohio University (1964).
12. B. Ronne, Proc. Easter School for Physicists I, 87 (1964) CERN Report.
13. J. P. Berge et al., Rev. Sc. Inst. 32, 538 (1961).
14. G. Campbell et al., J. Math. Phys. 8, 687 (1967).
15. A. Bigi et al., Nuovo Cimento 33, 1265 (1964).
16. J. W. Elbert et al., CERN Topical Conference on High Energy Collisions of Hadrons, Jan. 15, 1968.
17. J. M. Kohli, Nucl. Phys. B4, 443 (1968).
18. K. Imaeda, Nuovo Cimento 48A, 482 (1967).
19. Gradstein and Ryzhik, Table of Integrals, Series and Products, 316 (1965).
20. E. M. Friedlander, Nuovo Cimento 41A, 417 (1966).
21. F. Lehar et al., Nucl. Phys. B1, 199 (1965).
22. R. Hagedorn, Supp. Nuovo Cimento 3, 147 (1965).

23. R. Hagedorn, CERN Report TH/851 (1967).

24. M. A. Ijaz and J. Campbell, Nucl. Phys. B7, 175 (1968).

25. P. Berenyi, M. S. Thesis, Univ. of Toronto (1967).

26. M. A. Ijaz et al., Canadian Journal of Physics 46, 2663 (1968).

27. M. A. Ijaz and J. E. Campbell (Nuovo Cimento, to be published).

28. H. Drevermann et al., Phys. Rev. 161, 1356 (1967).

29. G. Goldhaber et al., Phys. Rev. 120, 300 (1960).

30. F. Bomse et al., Phys. Rev. 162, 1328 (1967).

31. N. Yeh, Columbia University, Private Communication.

32. M. Bardadin et al., Acta. Phys. Polon. 31 (1967).

33. M. Bardadin et al., Report No. 511/VI/PH/ Warsaw (1967).

34. K. Bockmann et al., Report No. P-837/VI/PH Warsaw (1967).

The vita has been removed from the scanned document

SIX PRONG EVENTS IN $\pi^- p$ INTERACTIONS AT 7.0 GeV/c

James E. Campbell

ABSTRACT

We have studied 2250 events with 6 charged tracks in the final state from 7.0 GeV/c $\pi^- p$ film taken at the BNL 80-inch bubble chamber. The events were fitted to the final states

$\pi^- p \rightarrow \pi^- \pi^- \pi^- \pi^+ \pi^+ p$	211 events	(1)
$\pi^- p \rightarrow \pi^- \pi^- \pi^- \pi^+ \pi^+ p\pi^0$	535 events	(2)
$\pi^- p \rightarrow \pi^- \pi^- \pi^- \pi^+ \pi^+ \pi^+ n$	230 events	(3)

We find the total six-prong cross section to be 2.40 ± 0.27 mb. The partial cross sections are: 0.22 ± 0.04 mb for reaction (1), 0.58 ± 0.09 mb for reaction (2), and 0.24 ± 0.05 mb for reaction (3).

Final state (1) shows significant $\rho(760)$ and $\Delta^{++}(1238)$ production. In reaction (2) there is $\Delta^{++}(1238)$ production and a bump at 1540 ± 20 MeV/c^2 with width 100 ± 40 MeV/c^2 in the $p\pi^0$ mass distribution (interpreted as $N^*(1520)$). The $\pi^+\pi^-\pi^+\pi^-$ mass plot shows peaks at 1085 ± 20 MeV/c^2 and 1470 ± 20 MeV/c^2 with widths 70 ± 30 MeV/c^2 and 60 ± 25 MeV/c^2. These peaks appear less prominently in reaction (3).

The transverse momentum distributions are analyzed in terms of statistical model predictions. In particular the Hagedorn statistical thermodynamical model gives temperatures of 120 MeV for pions and 150 MeV for nucleons.

The influence of Bose-Einstein statistics as found by Goldhaber is observed in the angles between pion pairs.